

**Piezoelectric Pressure Sensors as Switching Devices**

by

**Weibo Gao**

B.E., Xi'an Jiaotong University, P. R. China, 2017

Submitted to the Graduate Faculty of  
Swanson School of Engineering in partial fulfillment  
of the requirements for the degree of  
Master of Science in Mechanical Engineering

University of Pittsburgh

2019

UNIVERSITY OF PITTSBURGH  
SWANSON SCHOOL OF ENGINEERING

This thesis was presented

by

**Weibo Gao**

It was defended on

April 5, 2019

and approved by

Patrick Smolinski, Ph.D., Associate Professor, Department of Mechanical Engineering and  
Materials Science

Heng Ban, Ph.D., Professor, Department of Mechanical Engineering and Materials Science

Thesis Advisor: Qing-Ming Wang, Ph.D., Professor, Department of Mechanical Engineering and  
Materials Science

Copyright © by Weibo Gao

2019

# **Piezoelectric Pressure Sensors as Switching Devices**

Weibo Gao, M.S.

University of Pittsburgh, 2019

In this thesis, the applications where the piezoelectric pressure sensors using as switching devices were explored. To begin with, the piezoelectric pressure sensor was designed and manufactured. The piezoelectric Lead Zirconate Titanate (PZT) disks with customized thickness, fabricated by the tape-casting process, were used in this sensor as sensing element because of its great piezoelectric property. Two most widely used structure designs of the pressure sensors were compared and the PZT pressure sensor using unimorph structure was selected and manufactured. A unimorph structure model was established for the theoretical static and dynamic analysis of the pressure sensor. Based on the analysis, several pressure sensor samples with improved sensitivity and simple structure were manufactured. Using these pressure sensors, two experiments where the pressure sensors were used as switching devices were studied. For the first experiment, one pressure sensor was connected to an Arduino UNO board to form a trigger switch, which was designed to control a DC motor. By properly designing program algorithms and adjusting the control parameter, it is successfully realized to change the working state through touching the pressure sensor. As for the second experiment, a dimmer switch which consists of two pressure sensors were designed. The dimmer switch was also connected with the Arduino board to adjust the brightness of a dimmable LED. A brightness gradient was designed in the control program, which makes different brightness levels achievable by touching different positions on the dimmer switch.

## Table of Contents

<b>Preface.....</b>	<b>xi</b>
<b>1.0 Introduction.....</b>	<b>1</b>
<b>1.1 Fundamental Background of Piezoelectricity .....</b>	<b>1</b>
<b>1.2 Constitutive Equations of PZT Material .....</b>	<b>9</b>
<b>1.3 Different Constructions of Piezoelectric Sensors and Their Applications .....</b>	<b>14</b>
<b>1.3.1 Axial Sensors .....</b>	<b>15</b>
<b>1.3.2 Bending Sensors .....</b>	<b>18</b>
<b>1.4 Advantages and Disadvantages of Piezoelectric Pressure Sensors .....</b>	<b>19</b>
<b>1.5 Investigation on Current Commercial Piezoelectric Pressure Sensors .....</b>	<b>20</b>
<b>1.6 Research Objectives .....</b>	<b>21</b>
<b>2.0 Fabrication and Theoretical Analysis of PZT Piezoelectric Pressure Sensor .....</b>	<b>24</b>
<b>2.1 Fabrication and Polarization Process of The PZT Films.....</b>	<b>24</b>
<b>2.2 Design of the Pressure Sensor .....</b>	<b>28</b>
<b>2.2.1 Unimorph Structure .....</b>	<b>29</b>
<b>2.2.2 Bimorph Structure .....</b>	<b>30</b>
<b>2.3 Manufacturing of the Pressure Sensor .....</b>	<b>31</b>
<b>2.4 Theoretical Analysis on the Pressure Sensor .....</b>	<b>33</b>
<b>2.4.1 Static Response Analysis .....</b>	<b>34</b>
<b>2.4.2 Dynamic Response Analysis .....</b>	<b>43</b>
<b>3.0 Experimental Study on the Pressure Sensor as a Trigger Switch .....</b>	<b>46</b>

<b>3.1 Experimental Principle and Setup .....</b>	<b>46</b>
<b>3.1.1 Experimental Principle .....</b>	<b>46</b>
<b>3.1.2 Experiment Setup.....</b>	<b>51</b>
<b>3.2 Experimental Results and Analysis .....</b>	<b>52</b>
<b>4.0 Experimental Study of the Pressure Sensor as a Dimmer Switch.....</b>	<b>54</b>
<b>4.1 Experimental Principle and Setup .....</b>	<b>54</b>
<b>4.1.1 Experiment Principle .....</b>	<b>54</b>
<b>4.1.2 Experiment Setup.....</b>	<b>57</b>
<b>4.2 Experimental Results and Analysis .....</b>	<b>58</b>
<b>5.0 Conclusion and Future Work .....</b>	<b>61</b>
<b>5.1 Conclusion .....</b>	<b>61</b>
<b>5.2 Future Work .....</b>	<b>62</b>
<b>Appendix A Mathematica code for static response analysis.....</b>	<b>63</b>
<b>A.1 EXPANSION OF THE SYMBOLS USED IN THE STATIC ANALYSIS .....</b>	<b>63</b>
<b>Appendix B Control program for the two experiments .....</b>	<b>65</b>
<b>B.1 Control Program for experiment 1 .....</b>	<b>65</b>
<b>B.2 Control Program for experiment 2 .....</b>	<b>66</b>
<b>Bibliography .....</b>	<b>70</b>

## List of Tables

Table 1-1 Investigation on crucial parameters of current piezoelectric pressure sensor .....	21
Table 2-1 Properties of the PZT disks used for the pressure sensor.....	33
Table 3-1 Product specifications of the Power supply module.....	49

## List of Figures

Figure 1.1 Molecular model for explaining the direct piezoelectric effect.....	2
Figure 1.2 Piezoelectric phenomenon: (a) free charge flowing through the shorted circuit established on a piezoelectric material under pressure; (b) the stand state because of the removed pressure [1].....	3
Figure 1.3 Crystal structure of a typical piezoelectric ceramic: (a) the case where temperatures are above the Curie point; (b) the case where temperatures are below the Curie point .....	5
Figure 1.4 Polarizing process: (a)unpoled ceramic; (b) poling with DC electric field; (c) polarized .....	6
Figure 1.5 Effect of electric field on polarization and relative strain of a ceramic element: (a) hysteresis curve of polarization; (b) relative strain in direction of polarization [6] .....	7
Figure 1.6 Properties of a polarized piezoelectric ceramic element: (a) compressed: generated voltage has the same polarity as the polarization; (b) stretched: generated voltage has the polarity opposite to the polarization; (c) lengthened: applied voltage has the same polarity as the polarization; (d) shortened: applied voltage has the polarity opposite to the polarization .....	8
Figure 1.7 Linear relationship between the applied force and generated voltage .....	9
Figure 1.8 Axis nomenclature.....	10
Figure 1.9 Force-charge relationship of piezoelectric element: (a) d15 mode; (b) d31 mode; (c) d33 mode .....	13
Figure 1.10 Basic constructions of piezoelectric sensors: (a) axial sensor; (b) bending sensors .	14
Figure 1.11 Relationship between the force input and electrical output: (a) axial sensor; (b) bending sensor .....	15

Figure 1.12 The simplest accelerometer .....	16
Figure 1.13 Accelerometers in different designs: (a) center-mounted compression ; (b) Annual shear .....	17
Figure 1.14 Bending sensors in different configurarions: (a) series configuration ; (b) parallel configuration .....	18
Figure 2.1 Fabrication of PZT films: (a) Tape-casting process [16] ; (b) The fabricated PZT films .....	26
Figure 2.2 Electrodes coating: (a) The DC sputtering coater; (b) PZT films with partially covered electrodes .....	27
Figure 2.3 Polarizaiton and Measurment: (a) The polarization process; (b) The $d_{33}$ meter .....	27
Figure 2.4 A typical unimorph structure.....	29
Figure 2.5 A typical bimorph structure with the series configuration .....	30
Figure 2.6 Pressure Sensor Samples: (a) The fabricated PZT pressure sensor; (b) The voltage output response .....	32
Figure 2.7 The unimorph structure model .....	34
Figure 2.8 Two parts of the unimorph structure model .....	36
Figure 2.9 Sensitivity performance with different radius ratio and thickness ratio [23] .....	42
Figure 2.10 Equivalent model of the pressure sensor: (a) electric model; (b) mechanical model	43
Figure 2.11 Sensitivity of the sensor is a function of frequency .....	44
Figure 3.1 The block diagram of the whole system.....	47
Figure 3.2 The Arduino UNO board [26] .....	48
Figure 3.3 The Power Supply Module .....	50
Figure 3.4 The L293D IC chip.....	50

Figure 3.5 The Experiment Setup ..... 51

Figure 3.6 The Experiment Results: (a) The motor is turned on; (b) The motor is turned off ..... 52

Figure 4.1 The block diagram of the dimmer switch system..... 54

Figure 4.2 The simple supported bar model ..... 55

Figure 4.3 The design of the dimmer switch ..... 56

Figure 4.4 The experiment setup ..... 57

Figure 4.5 The experiment results: (a) left-end darkest mode; (a) middle moderate mode; (a) right-end brightest mode;..... 58

Figure 4.6 The brightness gradient ..... 59

## Preface

I would like to express my sincerest appreciation to my thesis advisor, Dr. Qing-Ming Wang, for all of his encouragement, support and guidance in this work and during the past two years of my M.S. study. I am very thankful to Dr. Heng Ban and Dr. Patrick Smolinski for their time and effort in reading and reviewing my thesis.

I am also extremely grateful to my research group members, Qiuyan Li, Alghamdi Saleh Awad and Mohammad Gudarzi for their help and encouragement in this research. Without these kind people, I would have never accomplished this work.

Special thanks to Dr. Zhi-Hong Mao who gave me very valuable advice on how to balance the research and life. Also, I'd like to thank to Dr. Xuefeng Bao, who let me to learn how to get along with people and to live a happy life in the United States.

Finally, I would like to express my deepest gratitude to my families and my girlfriend, Menghan Jiang, who are always supporting me and loving me in my life.

## **1.0 Introduction**

In this chapter, some basic concepts and theories on fundamental background of piezoelectricity and constitutive equations of PZT material are introduced in section 1.1 and 1.2, respectively. Then, focusing on sensors, the different constructions of piezoelectric sensors and their applications are illustrated in section 1.3. Further, the discussion on the advantages and disadvantages on the piezoelectric pressure sensors and an investigation on some pressure sensors products from the representative industries are made in section 1.4 and 1.5, respectively. Section 1.6 involves the research objectives of this thesis.

### **1.1 Fundamental Background of Piezoelectricity**

The word Piezoelectricity, coming from Greek, which means “electricity by pressure” (In Greek, Piezo is derived from pressure), was proposed by Hankel [1] in 1881 to name the phenomenon discovered by the Pierre and Jacques Curie brothers one year ago. In their experiments, by cataloging a number of crystals, such as tourmaline, quartz, topaz, cane sugar and Rochelle salt, they observed that positive and negative charges appeared on the crystal surfaces when subjecting the crystal to a mechanical force in different directions [2]. Tension and compression generate voltages of opposite polarity and the voltages is proportional to the applied force. The generation of an electric charge as the result of a force exerted on the material is named as “direct piezoelectric effect”.

Figure 1.1 shows a simple molecular model of a quartz crystal, which is to help explain the direct piezoelectric effect. At the beginning, there is no external force exerted on the quartz material, the three electric dipole moments are distributed at  $120^\circ$  angle between each other thus gravity centers of the negative and positive charges coincide. Therefore, these reciprocally cancelled negative and positive charges makes an electrically neutral molecule appears (Figure 1.1a). This internal reticular structure will be deformed when applying a force on the material, causing the separation of the positive and negative gravity center and generating little dipoles. Figure 1.1b shows the case where the stress applies along the z-direction and Figure 1.1c shows that along the x or y-direction, respectively.

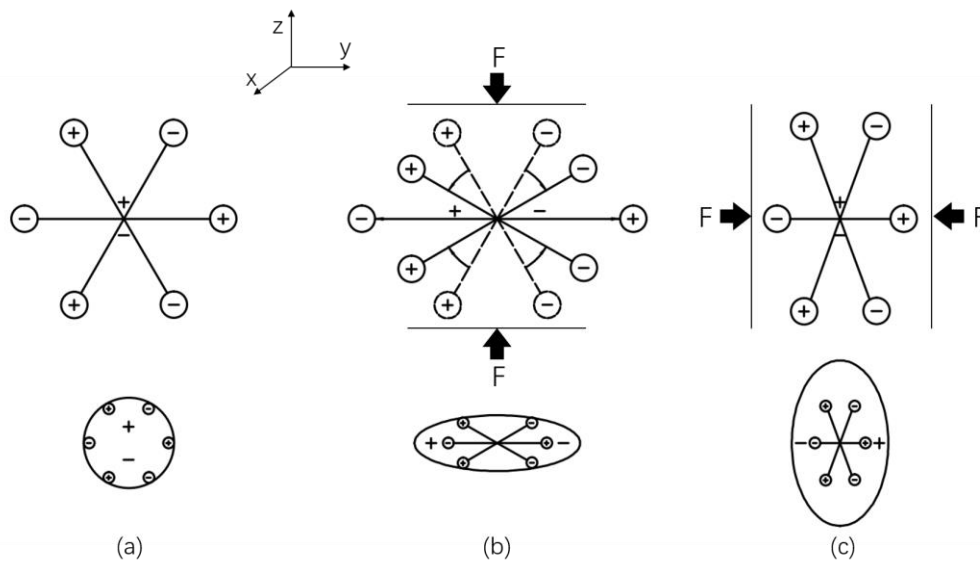


**Figure 1.1 Molecular model for explaining the direct piezoelectric effect**

Since the vector sum of the three electric dipole moments becomes nonzero, a distribution of a proportional charge appears in the material's surface. Therefore, the material is polarized. Especially, the x-direction is called the polarization direction for this crystal in that the charges are always generated along the x-axis no matter which axis the force is applied on. This polarization

can be utilized to transform the mechanical energy into electrical energy. For instance, the sensing applications, such as force or displacement sensors.

Figure 1.2a shows the piezoelectric material under pressure with two metal plated used as electrodes depositing on the surfaces where the positive and negative charges appears. Assuming that these electrodes are externally shorted through the wires that are connected to the galvanometer. Because of the direct piezoelectric effect, the polarization creates an electric field that causes the flow of free charge existing in the conductor. This free charge flow will remain until the free charge neutralizes the polarization. When the pressure on the crystal is removed, the polarization will disappear, and the free charge flow will reverse and return to the initial stand state (Figure 1.2b).

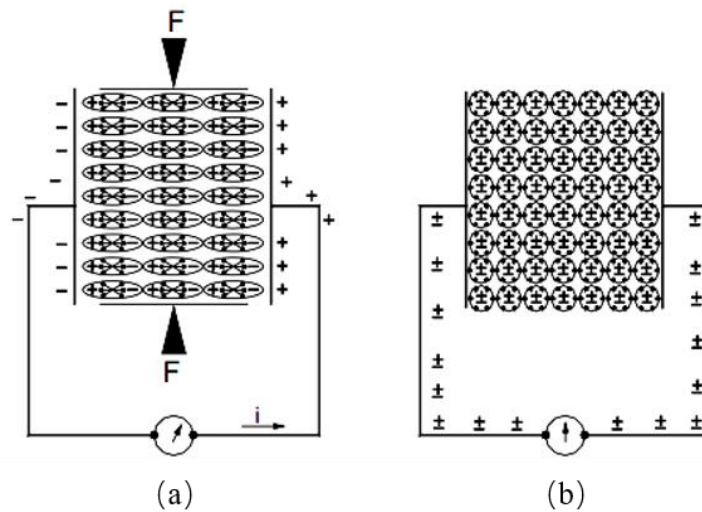


**Figure 1.2 Piezoelectric phenomenon: (a) free charge flowing through the shorted circuit established on a piezoelectric material under pressure; (b) the stand state because of the removed pressure [1]**

Just one year later, the Curie brother verified the existence of the reverse process that is predicted by Lippmann in 1881—"the inverse piezoelectric effect" [3]. That is, under similar circumstances, if such crystals are exposed to an electric field, they would experience an elastic

strain, and lengthened or shortened according to the polarity of the field, in proportion to the strength of the field. This strain can be utilized to transform the electrical energy into mechanical energy. Applications like motors and devices that precisely control positioning, and generating ultrasonic signals are widely used.

For many years, natural crystals such as tourmaline and quartz were the exclusive source of piezoelectric abilities, but only the piezoelectric have substantial advantage would they be accepted commercially or technically. This is the main reason why there was a long delay of technical break-through to large scale application for the piezoelectric materials. However, the avalanche of piezo technology starting in market was impossible until the realization that the mixed oxide compound barium titanite ( $\text{BaTiO}_3$ ) is a ferroelectric. In 1946,  $\text{BaTiO}_3$  ceramics were proved, which are easy to fabricate and shape at low price, can be fabricated by an electron polarization process to obtain the piezoelectric property [4]. Subsequently, researchers discovered that lead-zirconated-titanite materials exhibited greater sensitivity and higher operating temperatures, relative to  $\text{BaTiO}_3$  materials, “PZT” materials— $\text{Pb}[\text{Zr}_{(x)}\text{Ti}_{(1-x)}]\text{O}_3$ —replaced  $\text{BaTiO}_3$  materials in many applications and have become the most widely used piezoelectric ceramics [5].

The ferroelectric titanites can be hundreds of times more sensitive to electrical or mechanical input than natural materials because they exhibit different ferroelectric phases with only small energy differences, which results in the unusual combination of high dielectric permittivity in a strongly polar lattice in the broad vicinity of the phase boundaries. These conditions are critical to high piezoelectric constants and strong elasto-electric coupling. Because of the advantages of the ferroelectric titanites materials, since 1960s. man-made piezoelectric ceramics prepared from the ferroelectric titanites have replaced natural materials and have enabled the designers to explore the piezoelectric materials in many new applications.

A typical piezoelectric ceramic is a mass of perovskite crystals, each unit of which is composed of a small, tetravalent metal ion, usually titanium or zirconium, placed inside a lattice of larger divalent metal ions, usually lead or barium, and  $O^{2-}$  ions as shown in Figure 1.3a. Above a critical temperature, known as the Curie point, each perovskite crystal in the ceramic element exhibits a simple cubic symmetry with no dipole moment (Figure 1.3a). At temperature below the Curie point, however, each crystal has tetragonal or rhombohedral symmetry, depending on the composition of the material and, associated with that, a dipole moment (Figure 1.3b). Regions of like-oriented dipole moment called “domains”, and each domain carries a net dipole moment, and thus a net polarization. However, as shown in Figure 1.4a, the domains are randomly oriented because the direction of the dipoles is random in the element. Subsequently, the element has no overall polarization.

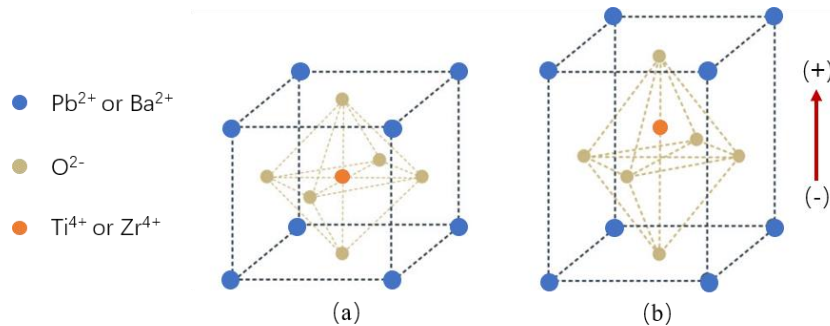


**Figure 1.3 Crystal structure of a typical piezoelectric ceramic: (a) the case where temperatures are above the Curie point; (b) the case where temperatures are below the Curie point**

The domains in a ceramic element are polarized (poled) by exposing it to a strong, direct current (DC) electric field, usually, but not exclusively, at a temperature slightly below the Curie temperature (Figure 1.4b). Through this polarizing treatment, domains most nearly aligned with the field, and the element expands (lengthens) in the direction of the electric field. When the electric field is removed, most of the dipoles are locked into a configuration of near alignment

(Figure 1.4c). Now the element has a permanent polarization, called the remnant polarization, and a permanent micrometer ranged elongation that make it anisotropic.

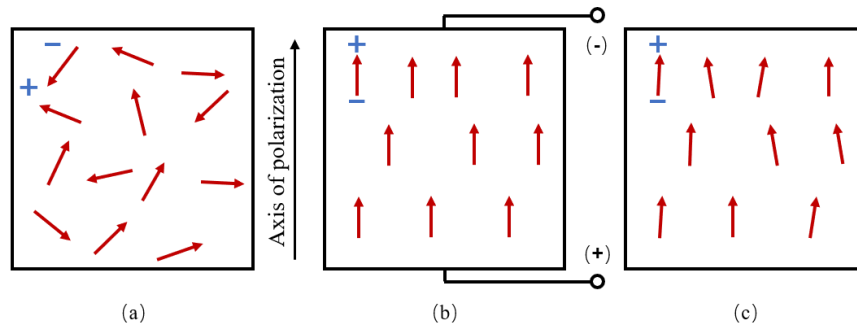


**Figure 1.4 Polarizing process: (a) unpoled ceramic; (b) poling with DC electric field; (c) polarized**

A polarized ferromagnetic material exhibits hysteresis, high and temperature dependent dielectric constants. By applying an electric field to a piezoelectric ceramic element, a typical hysteresis curve can be created as shown in Figure 1.5a.  $P_s$  is attained when this process reaches a saturation polarization and the remnant polarization can be determined by reducing the field to zero. Similarly,  $P_r$  can be reached by reversing the field to attain a negative saturation polarization and the same for the negative remnant polarization. Then, the positive remnant polarization is restored by reversing the field again. Below the hysteresis curve, the tracing in Figure 1.5b plots the relative change in the dimension of the ceramic element along the direction of polarization corresponding to the change in the electric field. The relative increase or decrease in the dimension parallel to the direction of electric field is accompanied by a corresponding, but for the relative increase or decrease in the dimension perpendicular to the electric field, it becomes approximately 50% smaller [6].

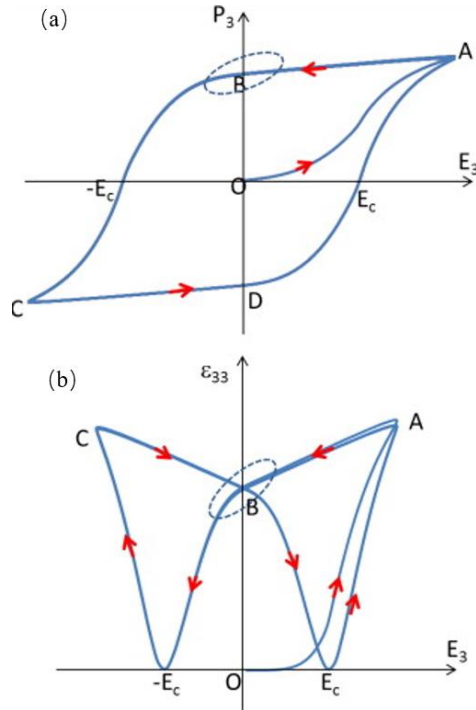


**Figure 1.5 Effect of electric field on polarization and relative strain of a ceramic element: (a) hysteresis curve of polarization; (b) relative strain in direction of polarization [6]**

The series of pictures in Figure 1.6 illustrated the properties of a polarized piezoelectric ceramic element. Mechanical compression or tension on a polarized piezoelectric ceramic element changes the dipole moments, thus creating a voltage. Compression along, or tension perpendicular to the direction polarization, generates voltage that has the same polarity as the poling voltage (Figure 1.6b). Relatively, Tension along, or the compression perpendicular to the direction polarization, generates voltage that has the opposite polarity as the poling voltage (Figure 1.6c). When operating in these generator actions, the piezoelectric ceramic element converts the mechanical energy into electrical energy. In this mode, the device is being used as a sensor or a generator, such as fuel-igniting devices and triggers, which is also one of the applications focused on in this thesis.

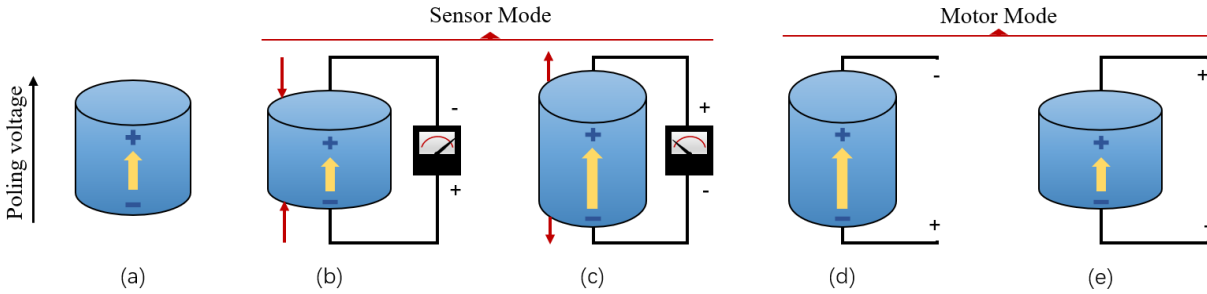


**Figure 1.6 Properties of a polarized piezoelectric ceramic element: (a) compressed: generated voltage has the same polarity as the polarization; (b) stretched: generated voltage has the polarity opposite to the polarization; (c) lengthened: applied voltage has the same polarity as the polarization; (d) shortened: applied voltage has the polarity opposite to the polarization**

If a voltage with the same polarity as the poling voltage is applied to a piezoelectric ceramic element, in the direction of the poling voltage, as shown in Figure 1.6d, the element will lengthen and its diameter will be smaller, according to the Poisson's effect. Relatively, by changing the polarity of the applied voltage, the element will shorten, and its diameter will expand (Figure 1.6e). Therefore, if an alternating voltage is applied on a piezoelectric ceramic element, the element will lengthen and shorten cyclically at the frequency of the alternating voltage, like a motor. When operating in these motor actions, the piezoelectric ceramic element converts the electrical energy into mechanical energy. In this mode, the device is being used as a motor or an actuator, such as buzzers, piezoelectric motors and ultrasound generating devices.

Additionally, as Figure 1.7 shows, the values for compression stress and the voltage generated by the applied force on the piezoelectric ceramic element are linearly proportional, up to a material-specific stress. This also works for the applied voltage and generated strain.

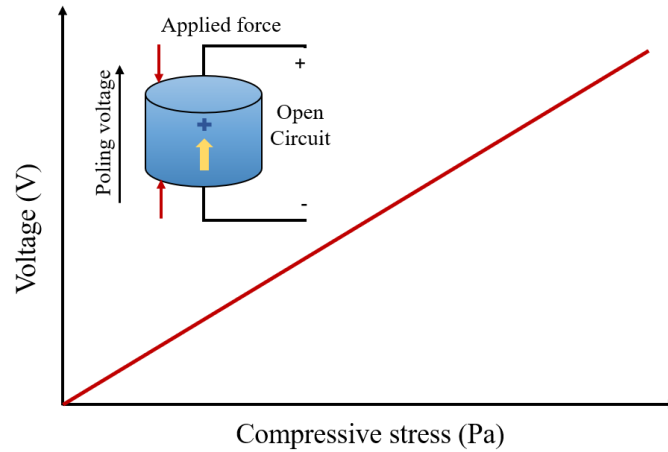


**Figure 1.7 Linear relationship between the applied force and generated voltage**

## **1.2 Constitutive Equations of PZT Material**

In this section, the three-dimensional form of the linear piezoelectric constitutive equations of PZT material will be introduced. Constitutive equations describing the electromechanical properties of piezoelectric materials are based on the assumption that the total strain in the transducer is the sum of the mechanical strain caused by mechanical stress and the controllable actuating strain caused by the applied voltage. Voigt [7] made the simplification of converting the description of stress and strain from three-dimension, second-rank tensors to six-dimension vectors by considering field tensors, such as temperature, electric displacement, stress and strain, and arranging the matter tensors relating them by their ranks, which describes the linear elasticity and piezoelectricity in a simple matrix form. Usually the direction of positive polarization of the piezoelectric ceramic element is considered as the Z-axis of a rectangular system of X, Y and Z axes. The axes X, Y and

Z are described by number subscript 1, 2 and 3, respectively, and shear about one of these axes is represented by number subscript 4, 5 and 6, respectively (Figure 1.8).

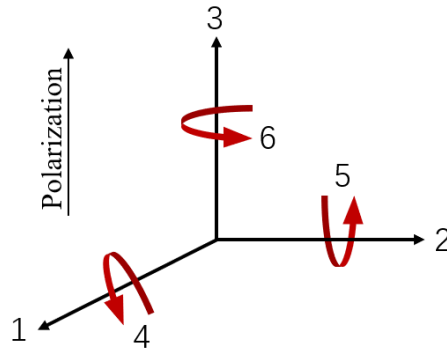


**Figure 1.8 Axis nomenclature**

The standard form of piezoelectric constitutive equation for a linear piezoelectric material can be commonly given in four sets as follows, depending on the physical structure under consideration. The prime denotes matrix transpose.

Homogeneous sets:

$$\begin{cases} S = s^E T + d' E \\ D = d T + \epsilon^T E \end{cases} \quad (1.1)$$

$$\begin{cases} T = c^D S - h' D \\ E = -h S + \beta^S D \end{cases} \quad (1.2)$$

Mixed sets:

$$\begin{cases} T = c^E S - e' E \\ D = e S + \epsilon^S E \end{cases} \quad (1.3)$$

$$\begin{cases} S = s^D T + g' D \\ E = -g T + \beta^T D \end{cases} \quad (1.4)$$

where

$S$  ... mechanical strain tensor

$T$  ... mechanical stress tensor

$D$  ... electric displacement  
 $E$  ... electric intensity  
 $c$  ... elastic stiffness tensor  
 $s$  ... mechanical compliance tensor  
 $\varepsilon$  ... dielectric permittivity tensor  
 $\beta$  ... impermeability tensor  
 $d$  ... piezoelectric strain tensor  
 $e$  ... piezoelectric stress tensor  
 $g$  ... piezoelectric voltage tensor  
 $h$  ... piezoelectric charge tensor

Considering the mechanical stress components and electric field components as independent variables, the equation 1.1, known as the coupled equation in the strain-charge form, is usually used as the constitutive equations for piezoelectric material. Therefore, the constitutive equations for a material of the 4mm crystal class (such as poled piezoelectric ceramic materials like PZT or BaTiO<sub>3</sub>) can be written as [8]:

$$\begin{bmatrix} S_1 \\ S_2 \\ S_3 \\ S_4 \\ S_5 \\ S_6 \end{bmatrix} = \begin{bmatrix} S_{11}^E & S_{12}^E & S_{13}^E & 0 & 0 & 0 \\ S_{21}^E & S_{22}^E & S_{23}^E & 0 & 0 & 0 \\ S_{31}^E & S_{32}^E & S_{33}^E & 0 & 0 & 0 \\ 0 & 0 & 0 & S_{44}^E & 0 & 0 \\ 0 & 0 & 0 & 0 & S_{55}^E & 0 \\ 0 & 0 & 0 & 0 & 0 & S_{66}^E = 2(S_{11}^E - S_{12}^E) \end{bmatrix} \begin{bmatrix} T_1 \\ T_2 \\ T_3 \\ T_4 \\ T_5 \\ T_6 \end{bmatrix} + \begin{bmatrix} 0 & 0 & d_{31} \\ 0 & 0 & d_{31} \\ 0 & 0 & d_{33} \\ 0 & d_{15} & 0 \\ d_{15} & 0 & 0 \\ 0 & 0 & 0 \end{bmatrix} \begin{bmatrix} E_1 \\ E_2 \\ E_3 \end{bmatrix} \quad (1.5)$$

$$\begin{bmatrix} D_1 \\ D_2 \\ D_3 \end{bmatrix} = \begin{bmatrix} 0 & 0 & 0 & 0 & d_{15} & 0 \\ 0 & 0 & 0 & d_{15} & 0 & 0 \\ d_{31} & d_{31} & d_{33} & 0 & 0 & 0 \end{bmatrix} \begin{bmatrix} T_1 \\ T_2 \\ T_3 \\ T_4 \\ T_5 \\ T_6 \end{bmatrix} + \begin{bmatrix} \varepsilon_{11} & 0 & 0 \\ 0 & \varepsilon_{22} & 0 \\ 0 & 0 & \varepsilon_{33} \end{bmatrix} \begin{bmatrix} E_1 \\ E_2 \\ E_3 \end{bmatrix} \quad (1.6)$$

The first equation here represents the relationship for the inverse piezoelectric effect and the latter for the direct piezoelectric effect. As mentioned before, the property of direct piezoelectric effect makes the piezoelectric transducer suitable for sensing application. In particular, if a mechanical stress field is applied on a PZT sensor, in open circuit case, assuming the applied electric field  $E$  is zero, by equation 1.6, the resulting electrical displacement becomes

$$\begin{bmatrix} D_1 \\ D_2 \\ D_3 \end{bmatrix} = \begin{bmatrix} 0 & 0 & 0 & 0 & d_{15} & 0 \\ 0 & 0 & 0 & d_{15} & 0 & 0 \\ d_{31} & d_{31} & d_{33} & 0 & 0 & 0 \end{bmatrix} \begin{bmatrix} T_1 \\ T_2 \\ T_3 \\ T_4 \\ T_5 \\ T_6 \end{bmatrix} \quad (1.7)$$

Then the generated charge  $q$  can be de obtained by

$$q = \iint [D_1 \quad D_2 \quad D_3] \begin{bmatrix} dA_1 \\ dA_2 \\ dA_3 \end{bmatrix} \quad (1.8)$$

Where the  $dA_1$ ,  $dA_2$  and  $dA_3$  are the differential of electrode areas in the 2-3, 1-3 and 1-2 planes, respectively.

Further, the generated voltage  $V_g$  is determined from

$$V_g = \frac{q}{C_p} \quad (1.9)$$

Where  $C_p$  is capacitance of the piezoelectric sensor. If a piezoelectric sensor consists of a PZT plate with two faces coated with thin electrodes layers, such as the sensor shown in Figure 1.8, and if the mechanical stress field is only applied along the 1-axis, the capacitance can be determined by

$$C_p = \frac{lw\epsilon_{33}}{t} \quad (1.10)$$

It can be seen from the equation 1.7 that, for the PZT material, there are only three distinct piezoelectric charge constants, which are  $d_{15}$ ,  $d_{31}$  and  $d_{33}$ . Corresponding to these piezoelectric

charge constants, different modes in 15, 31 and 33 direction are named  $d_{15}$  mode,  $d_{31}$  mode and  $d_{33}$  mode, respectively, as shown in Figure 1.9. Since the  $d_{15}$  mode is difficult to realize in a real structure because the 15 direction is the shear stress (Figure 1.9a), the  $d_{31}$  and  $d_{33}$  mode are widely used in the applications of force and pressure sensor. In sensing applications, the  $d_{31}$  mode represents that the direction of the applied mechanical stress is along the direction 1, which is perpendicular to the direction of polarization and charge collection (Figure 1.9b), whereas the  $d_{33}$  mode means that the applied mechanical stress is along the thickness, which is parallel to the direction of polarization and charge collections (Figure 1.9c).

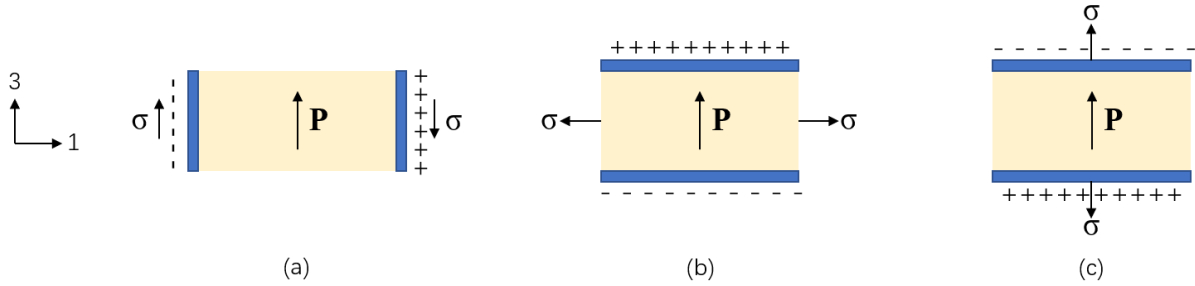


**Figure 1.9 Force-charge relationship of piezoelectric element: (a)  $d_{15}$  mode; (b)  $d_{31}$  mode; (c)  $d_{33}$  mode**

Therefore, as for the  $d_{31}$  mode, the generated voltage  $V_{g1}$  is found to be

$$V_{g1} = \frac{d_{31}T_1t}{\epsilon_{11}lt} = \frac{g_{31}T_1}{l} \quad (1.11)$$

Or

$$V_{g1} = \frac{d_{31}T_1t}{\epsilon_{11}wt} = \frac{g_{31}T_1}{w} \quad (1.12)$$

Meanwhile, as for the  $d_{33}$  mode, the generated voltage  $V_{g3}$  is determined by

$$V_{g3} = \frac{d_{33}T_3t}{\epsilon_{33}lw} = \frac{g_{33}T_3t}{lw} \quad (1.13)$$

Where the relationship between  $g$ ,  $d$  and  $\epsilon$  is

$$g = \frac{d}{\epsilon} \quad (1.14)$$

Through the equation 1.11 and 1.13, the proportional relationship between the external mechanical pressure and the generated voltage is verified again, as shown in the Figure 1.7. Based on this mechanism, as for the sensing applications, the external pressure sensed by a piezoelectric sensor which is connected with a proper interface can be obtained directly as a readable data.

### 1.3 Different Constructions of Piezoelectric Sensors and Their Applications

Generally, there are two basic constructions of piezoelectric sensors: axial sensors and bending sensors, as shown in Figure 1.10.

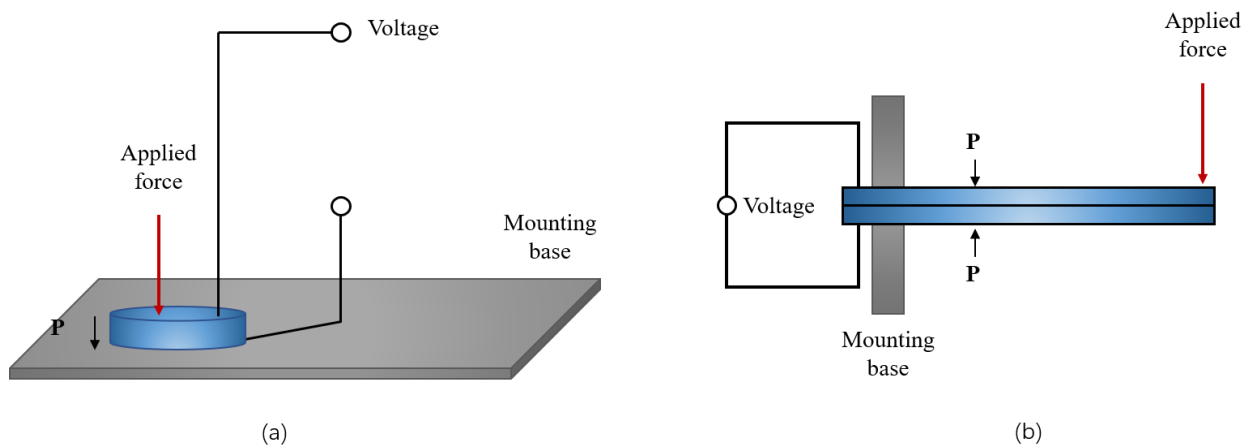


**Figure 1.10 Basic constructions of piezoelectric sensors: (a) axial sensor; (b) bending sensors**

### 1.3.1 Axial Sensors

A typical axial sensor senses the external force exerted parallel to the direction of the polarization of its piezoelectric ceramic element and generates the electrical energy signal such as voltage in the same direction (Figure 1.11a). Since both the mechanical stress and the generated electrical signal are expressed in direction 3, based on the concepts discussed in last section, thus the axial sensors are also named 33-mode sensors or  $d_{33}$  sensors. A typical bending sensor also senses the external force exerted in the same direction with the polarization of its ceramic element, however, because the force causes the piezoelectric ceramic element to bend along the plane that is perpendicular to the direction of the polarization, based on the discussion in last section, the bending sensors are also called 31-mode sensors or  $d_{31}$  sensors (Figure 1.11b). Further, because of the property that the piezoelectric ceramic element can be used both to sense the force signal and transit the output electrical signal, the  $d_{31}$  and  $d_{33}$  sensors are discussed in transducers [9].

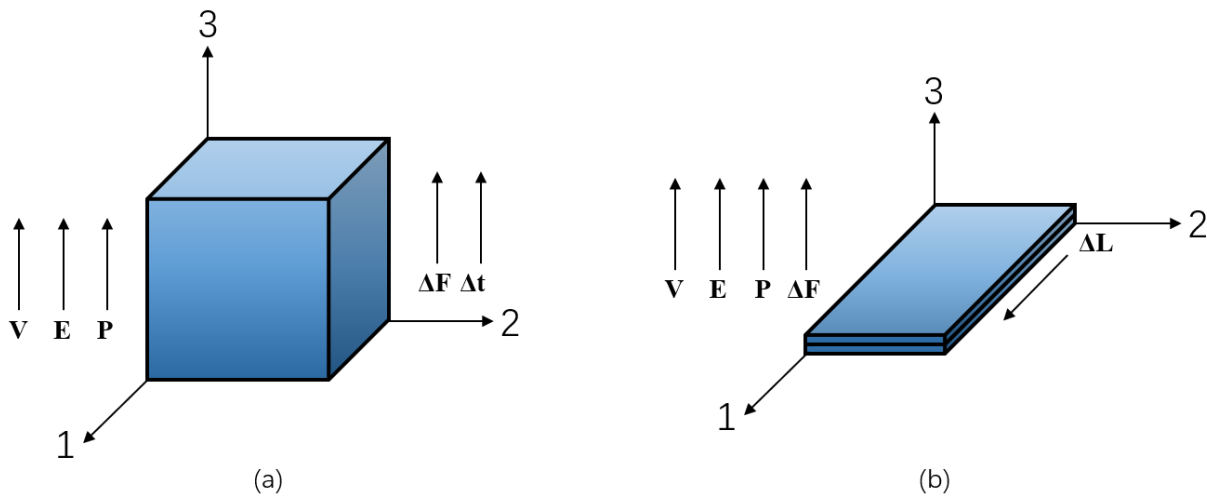
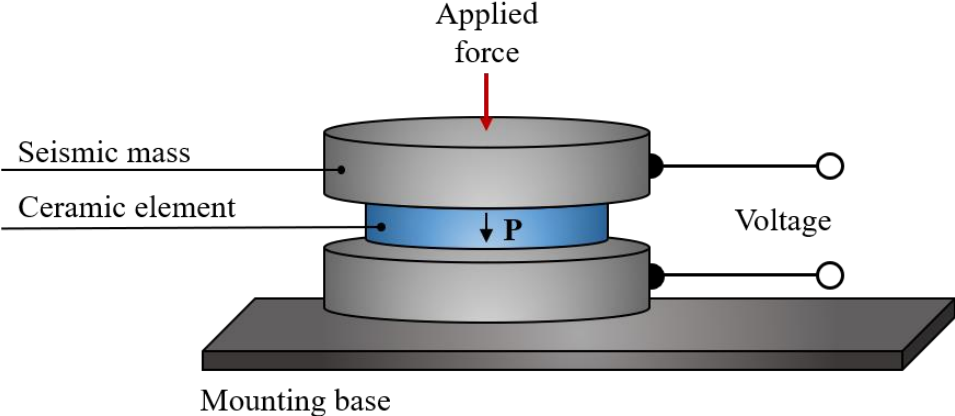


Figure 1.11 Relationship between the force input and electrical output: (a) axial sensor; (b) bending sensor

Basic applications for axial sensors include acceleration sensors (accelerometer), pressure sensor and force sensor. These axial sensors are similar in configurations and here the structure of the simplest accelerometer is used as an example for further study. As Figure 1.12 shows, the simplest accelerometer is made by securing a piezoelectric ceramic disk between an inactive seismic mass and a mounting base. The stress  $T$  induced by the force  $F$  exerted by the seismic mass on the piezoelectric ceramic element is determined by the surface area  $A$ , as well as the seismic mass  $M$  and the acceleration  $a$ , which can be expressed as

$$T = -\left(\frac{M}{A}\right) a$$



**Figure 1.12 The simplest accelerometer**

In practical applications, this simple compression accelerometer exhibits defects in stability and directional selectivity. However, some of these shortcomings are overcome by an alternative  $d_{33}$  mode design—the center-mounted compression accelerometer. As shown in Figure 1.13a, in this design, there is a ring-shaped piezoelectric ceramic element mounted around a cylindrical center column attached to the mounting base with a spring part above that. This relatively simple but robust and stable structure makes such kind of center-mounted compression

accelerometer suitable for shock and high-level measurement. However, even this design does not address the inherent error caused by temperature fluctuation. In fact, a temperature increase will create pyroelectric charges associated with the  $d_{31}$  and  $d_{33}$  mode, which are the electric effect of strain affiliated with temperature changes in polar materials and will disturb the measurement.

Because the center-mounted compression accelerometer does not eliminate all the error problems, another design named annular shear accelerometer that is capable of solving the problems caused by the thermal transients and maintaining highly reliable performance [10]. As Figure 1.13b shows, in this design, the tube shaped piezoelectric ceramic element, with the electrodes affixed on its face, is polarized axially and mounted around a center column. The seismic mass here is also a tube mounted around the piezoelectric ceramic element. The annular shear accelerometer, with such a construction design operated in  $d_{15}$  mode, is a balance in different properties such as wide frequency range, low sensitivity to directional selection and thermal inputs because it eliminates the pyroelectric charges. Therefore, such shear-based accelerometers are widely used in accelerometers.

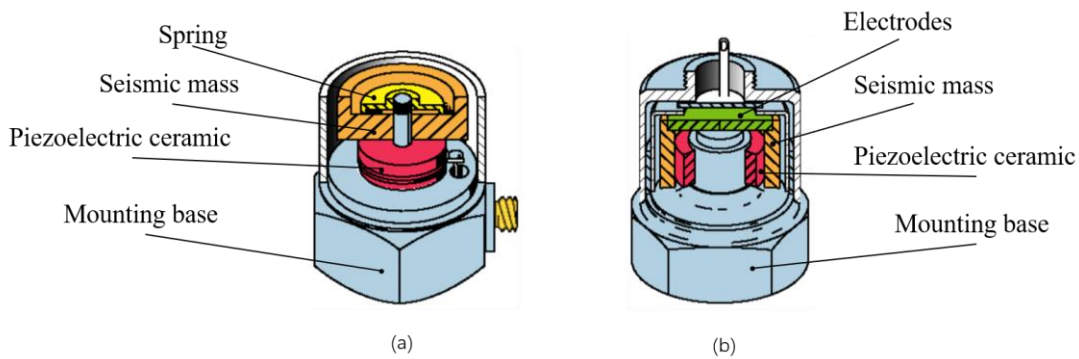


**Figure 1.13 Accelerometers in different designs: (a) center-mounted compression ; (b) Annual shear**

### 1.3.2 Bending Sensors

The Bending sensors are also called flexional sensors. As for a typical bending sensor, two plate or strip shaped piezoelectric ceramic element are bonded together to produce a flexible bilaminar element that is usually secured in a cantilever mounting. If the two plate or strip shaped element are configured together with the direction of polarization opposing and electrodes coating on their outer surface, as shown in Figure 1.14a, the sensor is in series configuration. However, if the two plate or strip shaped element are configured in the same direction as polarization, as Figure 1.14b shows, such a sensor is in parallel configuration.

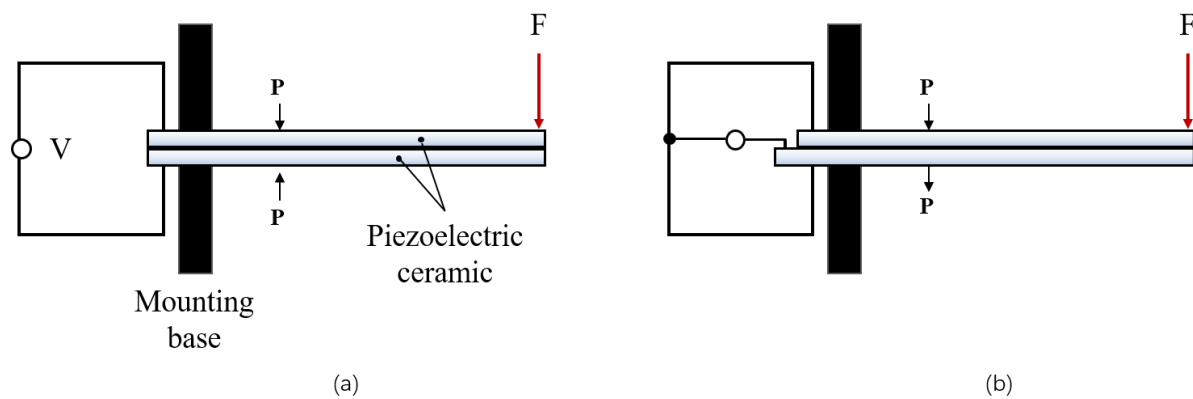


**Figure 1.14 Bending sensors in different configurations: (a) series configuration ; (b) parallel configuration**

When a perpendicular external force is applied on the free end of the flexional sensor to cause bending, tension will be introduced to the ceramic layer to which the external force is applied and compression will exist in the other layer, thus both layers will generate voltages. As for the bending sensor with a series configuration, the generated voltages have the same direction and the sum of the generated voltage by the two layers indicates the level of the force input. While in the case of parallel configuration, the generated voltages by the two layers are in the opposite direction,

which will cause a larger displacement. Usually, the bending sensor in series configuration is more preferred because of its simpler and more economic construction.

#### **1.4 Advantages and Disadvantages of Piezoelectric Pressure Sensors**

As discussed in the previous sections, since the mid-1960s, man-made piezoelectric ceramic materials have replaced natural crystal materials in many applications and have motivated many researchers to employ the direct and inverse piezoelectric effect in many new applications. Among these various applications, the pressure sensors, using the direct piezoelectric effect as their measuring principle, has obtained continued development over the decades and have been regarded as a mature technology with excellent reliability nowadays. The pressure sensors have been widely used in various applications including but not limited to turbines, precision plastic injection modeling, commercial electronics products and nuclear instrumentations [11].

Compared with pressure sensors using other mechanisms, there are several inherent advantages of piezoelectric pressure sensors. First, because the man-made piezoelectric ceramic materials can be easily fabricated and shaped at low price, the piezoelectric pressure sensor is available in desirable shape with low production cost and relatively compact size. Additionally, the stiffness of piezoelectric materials is approximately  $6.2 \times 10^{10} \text{ N/m}^2$ , which is similar to that of many metals and enables the piezoelectric materials to produce a high output with very little strain. In other words, piezoelectric sensing elements have essentially no deflection and are often referred to as solid state [12]. Thus, this property makes the piezoelectric pressure sensor has rugged construction, negligible phase shift and obtain extraordinary linearity over a wide amplitude range on the order of 120 dB.

The major disadvantage or limitation of piezoelectric pressure sensors is that it can only measure dynamic or changing pressure but not suitable for static pressure measurements, such as inertial guidance and barometric pressure measurements because the static pressure will result in an initial input signal that will decay slowly based on the affiliated electronics time constant of the piezoelectric ceramic material. In the first case, the time constant is based on the capacitance and resistance and corresponds to the first order high pass filter, which ultimately determines the measuring limit of the pressure sensor [12]. Besides, some  $d_{33}$  mode piezoelectric pressure sensors in relatively simple structure have high temperature sensitivity because their inherent error of thermal transit.

In summary, the piezoelectric pressure sensors are widely used in measuring dynamic pressures from turbulence, blast and engine combustions and so on because of the capabilities of fast response, ruggedness and extend measurement ranges.

### **1.5 Investigation on Current Commercial Piezoelectric Pressure Sensors**

Piezoelectrical pressure sensors, using the direct piezoelectric effect, are suitable for dynamic measurements with extended ranges. Additionally, their compact size makes the sensors can easily be integrated into the industrial applications and the ruggedness enable the sensors to work in extreme situations but maintain the measurement accuracy. After half-century development, as a mature technology, a variety of commercially available sensor products have emerged in the field of piezoelectric pressure sensors. In order to better understand the current development status of these products, an investigation on some crucial parameters of pressure sensor products has been done, as Table 1 shows. All these pressure sensors are commercially available and are from some

representative companies in the market, such as the CTS, BD SENSORS, PCB PIEZOELECTRONICS and KISTLER [12-15].

**Table 1-1 Investigation on crucial parameters of current piezoelectric pressure sensor**

Sample	Pressure Range (bar)	Sensitivity (pC/bar)	Operating temperature (°C)	Frequency (kHz)	Interface Circuit
BD-01	0-250	35	-40-400	85	NEEDED
BD-02	0-300	19	-40-400	170	NEEDED
BD-03	0-500	19	-50-120	170	NEEDED
CTS-01	0-2000	5.2	-50-200	240	NOT MENTIONED
PCB-01	0-100	50	-73-135	500	NEEDED
PCB-02	0-200	25	-73-135	500	NEEDED
PCB-03	0-500	10	-73-135	500	NEEDED
KS-01	0-250	37	-196-350	215	NEEDED
KS-02	0-250	37	-196-350	215	NEEDED

## 1.6 Research Objectives

As mentioned in previous sections, the PZT piezoelectric pressure sensors have several advantages such as rugged constructions, fast response, extended measurement ranges, compact size and easy shaping, which makes them very suitable for dynamic pressure response. However, according to

the investigation on some typical pressure sensors that are commercially available in last section, there are three major problems have been exposed: First, the sensitivity of current commercial piezoelectric pressure sensors can be further improved. Typical value range of sensitivity of the commercial pressure sensor can be found approximately as 16-35 pC/bar, based on the investigation, which means the current pressure sensor products does not explicit the potential advantage of sensitivity of piezoelectric materials. The sensitivity,  $S_v$  or  $S_Q$ , of a piezoelectric pressure sensor is the function of the electrical energy generated by the pressure sensor and the sensed mechanical pressure responsible for creating the electric energy. In an open circuit system,  $S_v$  is determined by the output voltage and pressure while in a short-cut circuit system,  $S_Q$  is determined by the generated charge and pressure. Besides, sensitivity also depends on the natural frequency of the piezoelectric ceramic element and their relationship will be discussed in detail in Section 3.3 later. Therefore, to obtain a better sensitivity, methods like optimization of the structure configuration of the pressure sensor such that the most sensitive part of the piezoelectric element can be employed and choosing the piezoelectric materials with better frequency and quality factor can be used.

Second, it can be seen that most commercial pressure sensors have a very complicated structure, which will not only result in the increase of the manufacturing cost but will also makes the maintenance and parts replacement become difficult to implement.

Last but not the least, according to the investigation in last section, it is found that many sensors have their own supplementary interface circuit in targeted and complex design with some crucial parts even not open-sourced for public. Though the design of the dedicated interface circuit could reduce the manufacturing cost in a certain extent, meanwhile the overall complexity and limitations of the whole pressure sensor system have increased.

Correspondingly, the research objective is to develop a piezoelectric pressure sensor system which has both the improved sensitivity and simple structure with a universal interface circuit, so that the three problems can be solved in a targeted manner. The research work can be divided into three parts:

The first part is to design and assemble the pressure sensor, which includes the fabricating process of the PZT films, structure design and the manufacturing of the pressure sensor.

The second part is the theoretical analysis of the pressure sensor, which includes the static response, dynamic response, determination of the boundary conditions, sensitivity, natural frequency and band width.

The third part is to develop a series of applications by connecting the pressure sensor with universal interface circuits.

## **2.0 Fabrication and Theoretical Analysis of PZT Piezoelectric Pressure Sensor**

In the previous sections, some fundamental concepts on piezoelectricity and properties of pressure sensors were reviewed. Since the research objective of this thesis is to develop a piezoelectric pressure sensor system which has both the improved sensitivity and simple structure with a universal interface circuit, “how to realize such a sensor” becomes the first focus. In this chapter, fabricating the PZT films, design and manufacturing the pressure sensor will be introduced in section 2.1, 2.2 and 2.3, respectively. Thereafter, the theoretical static and dynamic analysis based on the proposed pressure sensor will be discussed in section 2.4. The establishment of the whole sensing system and two applications of this system will be illustrated in the following sections.

### **2.1 Fabrication and Polarization Process of The PZT Films**

As mentioned in last section, man-made piezoelectric ceramic materials can be hundreds of times more sensitive to electrical or mechanical input than natural materials and are easy to fabricate and shape at low price. Among these piezoelectric ceramic materials, PZT has the highest piezoelectric coefficient and electrical-mechanical coupling coefficient, which makes this kind of material desirable in sensing applications. To use PZT in pressure sensors, the major challenge is to fabricate the PZT thick films with some flexibility that can withstand the bending load in some depth because the traditional PZT materials are so brittle that can only withstand very little bending deflection. However, tape-casting--recent development in the fabrication of PZT ceramic films by Lifeng Qin et al (2009) --makes the design and manufacturing of flexible piezoelectric pressure

sensors become possible because the thickness of fabricated PZT ceramic element can be controlled in several tens of micrometers by using the tape-casting process [16]. The tape-casting process can be briefly described as follows:

The first step is to prepare PZT ceramic powders with a Zr / Ti ratio of 52/48 and additives such as niobium oxide and lanthanum oxide. In order to form the PZT powders which has an average particle diameter in the submicron range, PbO, ZrO<sub>2</sub> and TiO<sub>2</sub> and other additives are mixed together by ball milling, then followed by drying, calcination and fine vibration grinding. These mixed PZT ceramic powders, organic binders and other organic additives, such as plasticizers, dispersants and deforming agents, constitute a slip for tape-casting.

About the binders, both aqueous and nonaqueous solvent can be used. For the aqueous binder system, a slurry was prepared by mixing the PZT powder (75 to 86 wt%) with a dispersant (1 to 2 wt%) and deionized water (13 to 124 wt%). Then, after a grinding process, the slurry was added to a dispersant (33% TRITON-100 solution in deionized water) and a wetting agent (33% TRITON CF-10) to form the milled slurry solution (85%), which was then added to the ammoniated 5310 and 5320 acrylic resins (7.5 wt% each) to form the slip for tape-casting [17]. As for the non-aqueous binder system, the binder mixture formulation consisted of 43 wt% binder polymer solution (acrylic resin), 54 wt% solvent and 3 wt% plasticizer. A binder mixture is added to the PZT powder to form the slip for tape-casting.

The next step is de-airing and casting. As shown in Figure 2.1a, By using the customized stainless steel belt-casting system, the de-aired PZT green tape sheet with various appropriate thickness (from 10 to 100  $\mu\text{m}$ ) was casted.

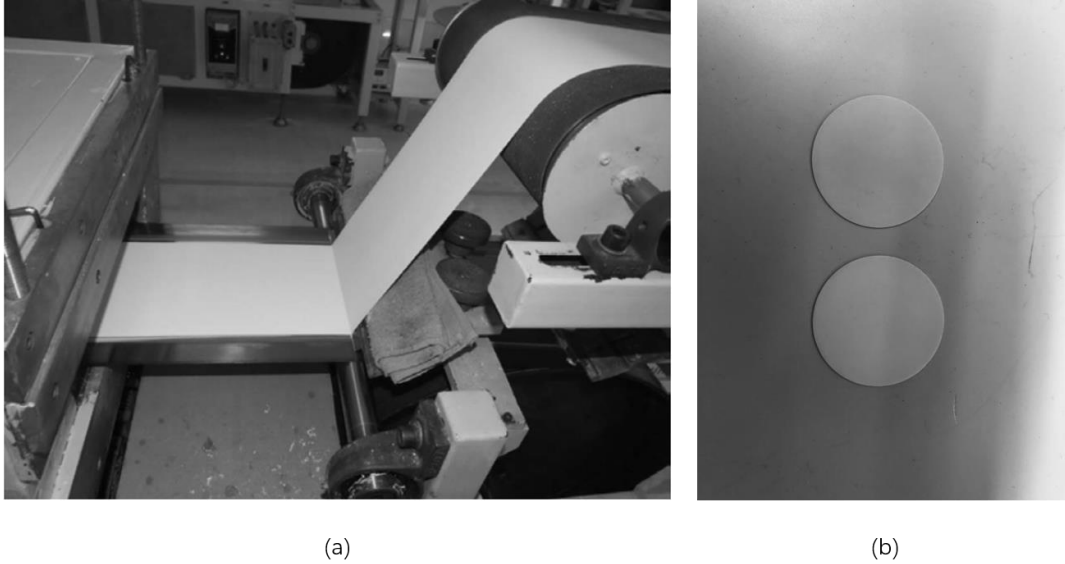
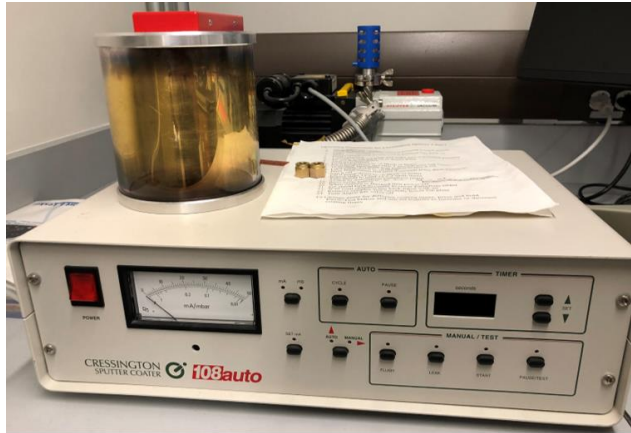


**Figure 2.1 Fabrication of PZT films: (a) Tape-casting process [16] ; (b) The fabricated PZT films**

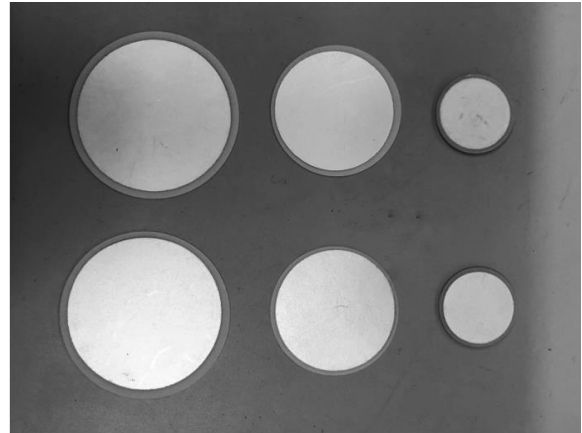
The last step is to shape the customized PZT element. The green sheets with the targeted thickness obtained in last process can be stamped or cut into the PZT elements with desired shape and size such as disk and rectangular, which was then burnout by a high-temperature binder around 500°C and sintered at a higher temperature, typically 1250 to 1300 °C, to form the final PZT ceramic film elements (Figure 2.1b). For the sake of compact sized design, in this thesis, the PZT ceramic elements used for the sensor manufacturing are all in a disk shape.

As mentioned in the previous sections, the ferroelectric titanites materials such as PZT will need an electron polarization process to obtain the piezoelectric properties. Therefore, after fabricating the PZT ceramic film elements, the next step is to coat the gold electrodes on the two surfaces of each of the PZT ceramic films and complete the polarization process.

As shown in Figure 2.2a, by using a DC sputtering coater, the thin gold electrodes can be coated on the PZT elements (Figure 2.2b).



(a)



(b)

**Figure 2.2 Electrodes coating: (a) The DC sputtering coater; (b) PZT films with partially covered electrodes**



(a)



(b)

**Figure 2.3 Polarization and Measurement: (a) The polarization process; (b) The  $d_{33}$  meter**

Since the process of coating electrodes is completed, as for the polarization, the PZT elements will be put in the silicone oil at a temperature of  $105^{\circ}\text{C}$  with a DC voltage connecting with the coated electrodes to apply the DC electric field across the z-direction of the PZT element for about half an hour (Figure 2.3a). After the polarization, the value of the piezoelectric charge constant  $d_{33}$  of each PZT element can be determined by properly clamping it on the  $d_{33}$  meter, as

shown in Figure 2.3b. In this thesis, the value of  $d_{33}$  of each PZT element used for sensor manufacturing is no less than 600.

## 2.2 Design of the Pressure Sensor

As discussed in section 1.2, the  $d_{31}$  and  $d_{33}$  mode are most widely used in the applications of force and pressure sensor. In  $d_{31}$  mode, the PZT element is bended along the z-direction or stretched in the x or y-direction because of the applied mechanical force which is parallel to the direction of the thickness (normal direction). The stress and strain along the transversal or planar direction are much larger than those in the z-direction, which brings a high sensitivity property to the piezoelectric element. However, as for the  $d_{33}$  mode, the stress and strain along the z-direction is directly proportional to the applied force that is in the direction of thickness, which will obtain a lower sensitivity compared to the  $d_{31}$  mode within the same thickness. Though a higher sensitivity can be reached by increasing the thickness of the PZT disk element, the flexibility that can withstand some bending deflection will be decreased. Since the objective of this thesis is to develop a piezoelectric pressure sensor system which has both the improved sensitivity and simple structure with a universal interface circuit, therefore, the design of the pressure sensor using  $d_{31}$  mode will be adopted in this thesis. A circular diaphragm is a common structure in  $d_{33}$  mode for dynamic pressure sensors with the uniform pressure loading applied on it. In the past few decades, a great amount of research on investigating the properties of different types of PZT piezoelectric transducers has been conducted and the most widely used structure of these devices are the unimorph and bimorph structure [18-22].

### 2.2.1 Unimorph Structure

A typical unimorph structure, as shown in Figure 2.4, consists of a PZT disk partially covered on a metal or polymer substrate whose diameter is slightly larger than that of the PZT disk. These two parts are bonded together by the Epoxy binder. The generated charges due to the exerted pressure can be picked up by wires connected to the electrodes coating on the upper and lower surfaces of the PZT disk.

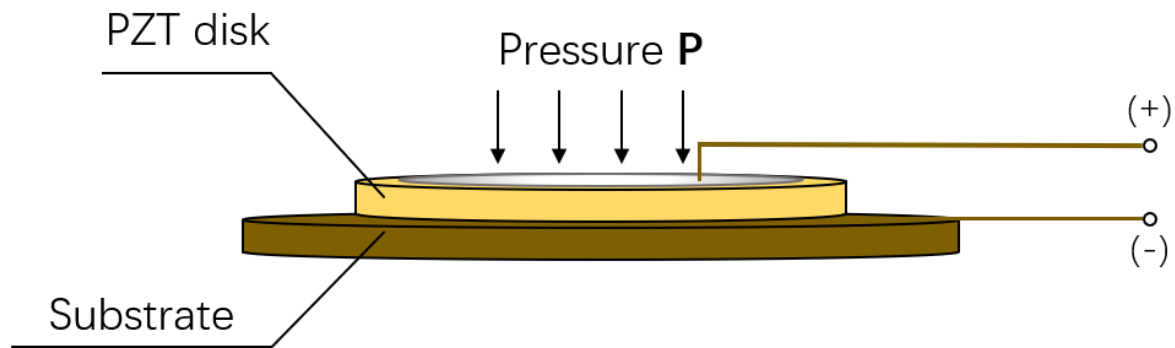


Figure 2.4 A typical unimorph structure

In this unimorph structure, if a perpendicular dynamic uniform pressure exerts on the upper surface of the PZT disk, with the boundary of the substrate clamped, the sensor will have a bending deflection and then generate charges on the PZT disk. Assuming that the bending deflection is far less than the thickness of the PZT disk, according to the small bending elastic theory, the generated charges harvested in the open circuit would be proportional to the amplitude of the mechanical pressure.

The unimorph structure has lots of advantages of high sensitivity, simple structure and robust reliability and so on, which makes it suitable for the further experiments discussed in the later sections.

## 2.2.2 Bimorph Structure

As discussed in section 1.3, according to the differences between the direction of the configuration and the polarization of the two PZT disks, the bimorph structured can be divided into the series configuration and the parallel configuration. Here the series configured bimorph structure was used as an example, as Figure 2.5 shows. Two PZT disks are bonded together by the epoxy with the direction of polarization opposing and electrodes coating on their outer surface.

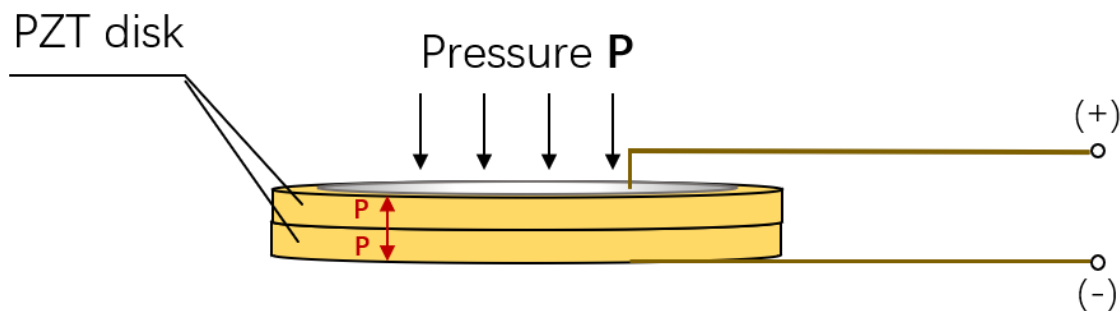


**Figure 2.5 A typical bimorph structure with the series configuration**

In the bimorph structure with a series configuration, when a perpendicular dynamic pressure is applied on the upper face of the sensor to cause bending, contraction will be introduced to the upper PZT disk where the external force is applied and expansion will exist in the lower PZT disk, thus both layers will generate voltages that have the same direction and the sum of the generated voltage by the two layers would be proportional to the amplitude of the mechanical pressure. In this way, the bimorph structure can obtain a larger sensitivity than that of the unimorph, thus it can be used in the sensing application where the force or pressure input can be relatively small. However, since the bimorph structure only consists of two PZT elements without any metal substrate, the increased thickness and the exposed PZT ceramic element make the bimorph structure more fragile than the unimorph. Usually, the bimorph structure is used in strip-shaped

PZT elements to form such a PZT cantilever bender that are more flexible but not the disk-shaped ones.

Therefore, based on the research objective of this thesis and the two applications case in the later sections, the unimorph structure was chosen for the further manufacturing process and theoretical analysis in the later sections.

### **2.3 Manufacturing of the Pressure Sensor**

In this thesis, the PZT disk with diameter in 12.5 mm and thickness in 0.25 mm will be used for the manufacturing of the pressure sensor in unimorph structure and the full properties of the PZT sample and the sensors will be listed at the end of this section. The manufacturing process is shown as the following steps:

First, take one PZT disk sample that has been polarized through the process in section 2.1 then properly clamped it on the  $d_{33}$  meter. After recording the number shown on the  $d_{33}$  meter, the polarity of the PZT sample can also be determined.

Second, according to the polarity of the PZT disk sample, use the silver conductive epoxy (MG chemicals 8831) to stick the copper wires on the upper (corresponding to the positive side) and lower (corresponding to the negative side) surfaces of the PZT disk, respectively. The silver epoxy should be applied as smoothly as possible on the surfaces of the disk so that it will not only fully cover the copper wire to ensure the wires are connected to the electrodes coated on the PZT disk but also to make the surface of the PZT part become flat enough, especially for the lower surface, to avoid the interspace between the disk and the substrate. Since it usually needs 10 to 15

minutes to completely dry the silver epoxy, wait until the epoxy on the previous side is completely dry and then apply it to the other side.

Third, while waiting the drying process of the PZT disk, use a manual hole-punch tool to stamp the substrate for the pressure sensor. A copper sheet with the thickness of 0.15 mm was used for the substrate and it was punched into several 15 mm diameter copper disk, considering that the diameter of the substrate should be a slightly larger than that of the PZT disk.

Next, when the silver epoxy on both surfaces of the PZT disk is completely dry, drop a moderate amount of Polyimide epoxy (Devcon 2 Ton 14310) on the center of the copper substrate. Then stick the lower surface of the PZT disk to the copper substrate with their center coinciding as much as possible to ensure the balance of the whole structure.

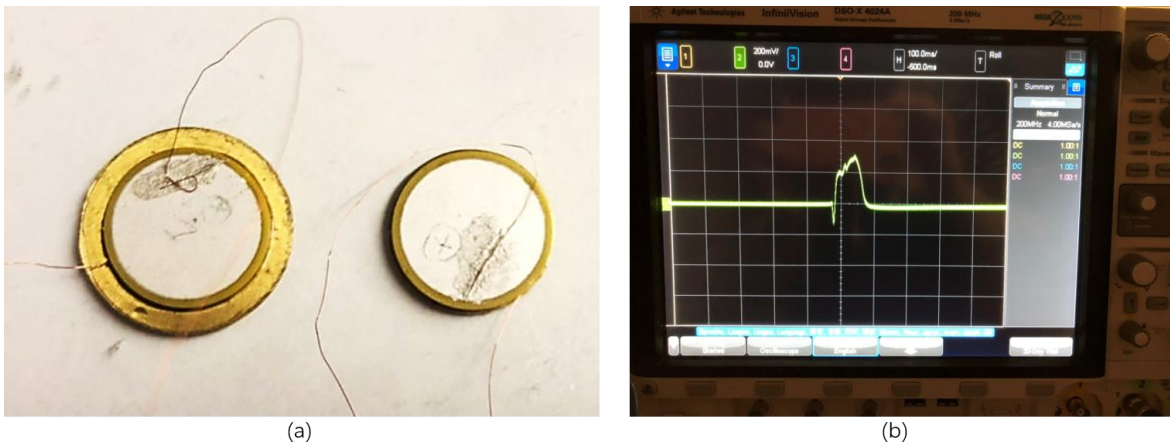


**Figure 2.6 Pressure Sensor Samples: (a) The fabricated PZT pressure sensor; (b) The voltage output response**

Finally, connect the manufactured PZT pressure sensor (Figure 2.6a) in unimorph structure with the oscilloscope for data recording of the sample testing. The positive pin should be connected to the red input signal line while the negative pin should be connected to the black ground wire. Then, use the finger to press the pressure sensor to introduce an approximate pulse input and check

if the oscilloscope shows an ideal voltage output signal response, as shown in Figure 2.6b, which means the manufactured PZT pressure sensor can be applied on the further applications.

The properties of the PZT disks used for the pressure sensor are shown in Table 2-1.

**Table 2-1 Properties of the PZT disks used for the pressure sensor**

Resonant Frequency (KHz)	160±10
Electrostatic capacitance (nF)	11±30%
Pass band width ( $\Delta f/f_r\%$ )	$\geq 18\%$
Piezoelectric ceramic disk diameter (mm)	12.5±0.30
Piezoelectric ceramic disk thickness (mm)	0.25±0.02
Piezoelectric strain constant $d_{33}$	$\geq 600$

#### **2.4 Theoretical Analysis on the Pressure Sensor**

As discussed in section 2.1, the unimorph structure is chosen for the theoretical analysis in this section, including the theoretical response analysis and dynamic response analysis. As for the theoretical response analysis, an analytical approach for modeling a simply supported piezoelectric pressure sensor in unimorph structure will be discussed. For the dynamic analysis, by establishing an equivalent electric circuit model of the pressure sensor, the dynamic equation which describes the relationship between the generated voltage and the applied pressure will be derived. Besides, the sensitivity of the sensor will be also discussed.

### 2.4.1 Static Response Analysis

The unimorph structure model with a simply supported boundary condition is established to satisfy the limitations in the applications that the PZT disk is only on one side of the substrate, as shown in Figure 2.7. Assuming that the PZT disk is perfectly bonded to the substrate and the thickness of the epoxy binder is negligible.  $h_p$  and  $h_s$  represent the thickness of the PZT disk layer and the copper substrate layer, respectively.  $Z_c$  describes the distance from the interface of the two layers to the neutral axis. The radius of the PZT disk is  $R_p$  while the radius of the substrate is a little bit larger the PZT disk, which is represented by  $R_s$ .

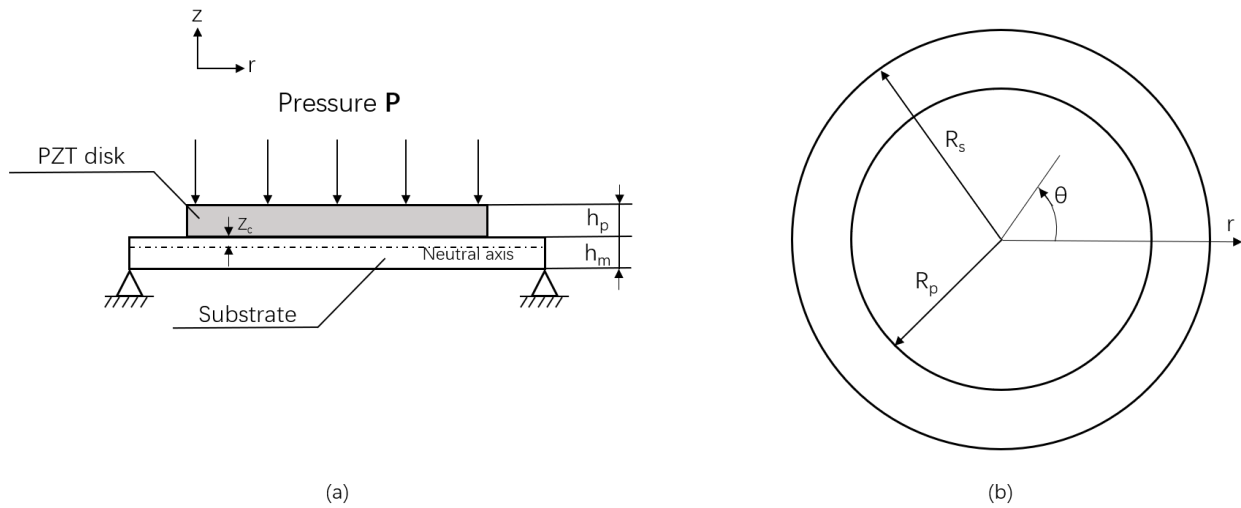


**Figure 2.7 The unimorph structure model**

The energy method is used to describe the total energy in a pressure-loaded piezoelectric plate and ultimately calculate the charge generated by the pressure source.

In order to describe the total energy in the piezoelectric disk subjecting to the pressure and calculate the charges generated by the pressure, an electromechanical coupling analysis is conducted followed by the previous work done by Mo et al (2010) [23].

Vinson (1974) [24] derived the equation which governs the bending, transverse deflection and shearing action of the disk subjected to uniformly distributed constant pressure load P, as shown in equation 2.1-2.4.

$$\nabla^4 W_r = \frac{1}{r} \frac{\partial}{\partial r} \left( r \frac{\partial}{\partial r} \left( \frac{1}{r} \frac{\partial}{\partial r} \left( r \frac{\partial W_r}{\partial r} \right) \right) \right) = \frac{P}{D} \quad (2.1)$$

$$M_r = -D \left( \frac{\partial^2 W_r}{\partial r^2} + \frac{\nu}{r} \frac{\partial W_r}{\partial r} \right) \quad (2.2)$$

$$M_\theta = -D \left( \frac{1}{r} \frac{\partial W_r}{\partial r} + \nu \frac{\partial^2 W_r}{\partial r^2} \right)$$

$$Q_r = -D \frac{\partial}{\partial r} \left( \frac{1}{r} \frac{\partial}{\partial r} \left( r \frac{\partial W_r}{\partial r} \right) \right) \quad (2.3)$$

Where

$W_r$  ... deflection of the disk in the z-direction

$r$  ... distance from the center of the disk to the point of deflection

P ... applied pressure

$D$  ... flexural rigidity of the sensor

$M_r$  ... moments in the radius direction

$\nu$  ... Poisson's ratio

$M_\theta$  ... moments in the angular direction

As Figure 2.8 shows, the unimorph structure model is divided into two parts. One is the inner part consisting the PZT disk and part of the substrate, where  $r \leq R_p$ . The other is the outer part which consists the rest of the substrate, where  $R_p < r \leq R_s$ . Therefore, substituting the boundary conditions at  $r=0$  and the two simply supported edge, three constants can be found as follows

$$W_r = M_r = 0 \text{ (when } r = R_s), \quad \frac{dW_r}{dr} = \lambda \text{ ( } r = 0) \quad (2.4)$$

Where  $\lambda$  represents a finite value.

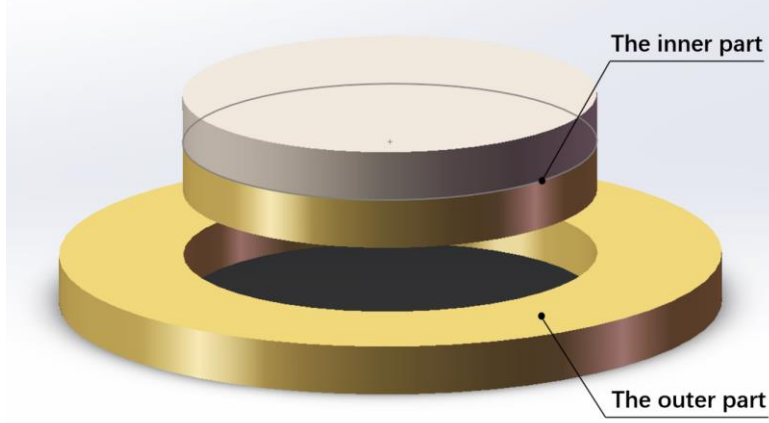


**Figure 2.8 Two parts of the unimorph structure model**

Besides, considering the boundary conditions at the interface of the two parts, where  $r = R_p$ , other four relationships can be obtained

$$W_r^i = W_r^o \text{ (when } r = R_p) \quad (2.5)$$

$$\begin{cases} W_r^i = W_r^o, \\ M_r^i = M_r^o, \\ Q_r^i = Q_r^o, \\ \frac{dW_r^i}{dr} = \frac{dW_r^o}{dr} \end{cases} \quad (2.6)$$

Where the superscripts i and o represent the inner and the outer part, respectively.

Therefore, the deflection of the inner and outer part in the z-direction can be written as  $W_r^i$  and  $W_r^o$  and their general solutions can be obtained as

$$W_r^i = \frac{P_0 r^4}{64D_i} + C_2 r^2 + C_1 \quad (2.7)$$

$$W_r^o = \frac{Pr^4}{64D_o} + C_5r^2 + C_4 \ln r + C_3 \quad (2.8)$$

Where  $C_1 - C_5$  can be found in the **Appendix A** and  $D_i$  and  $D_o$  are the flexural rigidity of the inner and outer part, which can be obtained by

$$D_i = \frac{E_i(h_p + h_s)^3}{12(1 - \nu_i)} \quad (2.9)$$

$$D_o = \frac{E_o h_s^3}{12(1 - \nu_o)} \quad (2.10)$$

Here  $E$  is the Young's modulus. Additionally, because the outer part only consists of the substrate, For the same parameter symbol, its value of the outer part should be equal to that of the substrate. For example, the Poisson's ratio  $\nu_o$  should be equal to  $\nu_s$ . However, since the inner part consists both the PZT disk and its bonded substrate, the Young's modulus  $E_i$  and the Poisson's ratio  $\nu_i$  can be determined by following Christensen's work [25], where

$$E_i = \frac{h_p}{h_p + h_s} E_p + \frac{h_s}{h_p + h_s} E_s + \frac{h_p h_s E_p E_s (\nu_p - \nu_s)^2}{(h_p + h_s) h_p E_p (1 - \nu_s^2) + (h_p + h_s) h_s E_s (1 - \nu_i^2)} \quad (2.11)$$

$$\nu_i = \frac{h_p \nu_p E_p (1 - \nu_s^2) + h_s \nu_s E_s (1 - \nu_p^2)}{h_p E_p (1 - \nu_s^2) + h_s E_s (1 - \nu_i^2)} \quad (2.12)$$

Similarly, the subscripts  $p$  and  $s$  indicate the PZT disk and substrate, respectively.

Next, to solve the moment equation, the relationship between the strain  $\varepsilon$ , the stress  $\sigma$  of the sensor should be determined. Recall the constitutive equations discussed in section 1.2, which can be rewritten in the polar coordinate system as following. The prime denotes the matrix transverse and the subscript  $r$  is used for describing the radius direction and  $\theta$  is for the angular direction.

$$\varepsilon_{ri} = S_{11}^E (\sigma_{ri} - \nu_i \sigma_{\theta i}) - d_{31} E_3 \quad (2.13)$$

$$\varepsilon_{\theta i} = S_{11}^E (\sigma_{\theta i} - \nu_i \sigma_{ri}) - d_{31} E_3$$

$$\varepsilon_{ro} = S_{11}^E(\sigma_{ro} - \nu_o\sigma_{\theta o}) \quad (2.14)$$

$$\varepsilon_{\theta o} = S_{11}^E(\sigma_{\theta o} - \nu_o\sigma_{ro})$$

$$D_3 = -d_{31}(\sigma_{ri} + \sigma_{\theta i}) + \varepsilon'_{33}E_3 \quad (2.15)$$

Where

$S_{11}^E$  ... the elastic compliance constant of the PZT material

$d_{31}$  ... piezoelectric charge constant

$E_3$  ... the electric field strength in direction 3

$D_3$  ... the charge density in direction 3

$\varepsilon_{33}$ ... permittivity of the piezoelectric

As for the inner part, the stress in the piezoelectric disk can be determined by

$$\sigma_{rip} = \frac{(\varepsilon_{ri} + \nu_p\varepsilon_{\theta i} + (1 + \nu_p)d_{31}E_3)}{S_{11}^E(1 - \nu_p^2)} \quad (2.16)$$

$$\sigma_{\theta ip} = \frac{(\nu_p\varepsilon_{ri} + \varepsilon_{\theta i} + (1 + \nu_p)d_{31}E_3)}{S_{11}^E(1 - \nu_p^2)} \quad (2.17)$$

And for the stress in the substrate of the inner part

$$\sigma_{ris} = \frac{(\varepsilon_{ri} + \nu_s\varepsilon_{\theta i})}{S_s(1 - \nu_s^2)} \quad (2.18)$$

$$\sigma_{\theta is} = \frac{(\nu_s\varepsilon_{ri} + \varepsilon_{\theta i})}{S_s(1 - \nu_s^2)} \quad (2.19)$$

Where  $S_s$  is the he elastic compliance constant for the substrate, which is equal to the reciprocal of its Young's modulus.

Further, as for the outer, the stress in the rest of the substrate can be determined by

$$\sigma_{ros} = \frac{(\varepsilon_{ro} + \nu_s\varepsilon_{\theta o})}{S_s(1 - \nu_s^2)} \quad (2.20)$$

$$\sigma_{\theta os} = \frac{(v_s \varepsilon_{ro} + \varepsilon_{\theta o})}{S_s(1 - v_s^2)} \quad (2.21)$$

On the other hand, since the strains of the two parts can be determined by the curvature  $\kappa$  and the distance from to the neutral axis, equation 2.13 and 2.14 can also be written as

$$\varepsilon_{ri} = \kappa_{ri}(z - z_c) \quad (2.22)$$

$$\varepsilon_{\theta i} = -\kappa_{\theta i}(z - z_c) \quad (2.23)$$

$$\varepsilon_{ro} = -\kappa_{ro}(z - z_c) \quad (2.24)$$

$$\varepsilon_{\theta o} = -\kappa_{\theta o}(z - z_c) \quad (2.25)$$

Where  $\kappa_{ri}$ ,  $\kappa_{\theta i}$ ,  $\kappa_{ro}$  and  $\kappa_{\theta o}$  can be referred to the **Appendix A** and  $z_c$  can be obtained by

$$z_c = \frac{h_p^2 S_m R_p - h_s^2 S_{11}^E R_s}{2(S_{11}^E h_s R_s + S_m h_p R_p)} \quad (2.26)$$

Therefore, substituting the equations 2.13-2.25 in to the equation 2.2 and equation 2.3, the moment equations can be rewritten as following

$$\begin{aligned} M_{ri} = & \int_0^{h_p} \left( \frac{(\varepsilon_{ri} + v_p \varepsilon_{\theta i} + (1 + v_p) d_{31} E_3)}{S_{11}^E (1 - v_p^2)} \right) (z - z_c) dz \\ & + \int_{-h_s}^0 \frac{(\varepsilon_{ri} + v_s \varepsilon_{\theta i})}{S_s (1 - v_s^2)} (z - z_c) dz \end{aligned} \quad (2.27)$$

$$\begin{aligned} M_{\theta i} = & \int_0^{h_p} \left( \frac{(v_p \varepsilon_{ri} + \varepsilon_{\theta i} + (1 + v_p) d_{31} E_3)}{S_{11}^E (1 - v_p^2)} \right) (z - z_c) dz \\ & + \int_{-h_s}^0 \frac{(v_s \varepsilon_{ri} + \varepsilon_{\theta i})}{S_s (1 - v_s^2)} (z - z_c) dz ; \end{aligned} \quad (2.28)$$

$$M_{ro} = \int_{-h_s}^0 \frac{(\varepsilon_{ro} + v_s \varepsilon_{\theta o})}{S_s (1 - v_s^2)} (z - z_c) dz \quad (2.29)$$

$$M_{\theta o} = \int_{-h_s}^0 \frac{(v_s \varepsilon_{ro} + \varepsilon_{\theta o})}{S_s (1 - v_s^2)} (z - z_c) dz \quad (2.30)$$

Finally, the relationship between the generated charges and the mechanical pressure can be determined by the energy equation. Similarly, the energy equations for the inner part and outer part are also different and will be discussed respectively.

As for the inner part, the energy of a volume element of the PZT disk can be obtained by

$$dU_{ip} = \frac{1}{2} \varepsilon_{ri} \sigma_{rip} + \frac{1}{2} \varepsilon_{\theta i} \sigma_{\theta ip} + \frac{1}{2} D_3 E_3 \quad (2.31)$$

For the substrate of the inner part, it becomes

$$dU_{is} = \frac{1}{2} \varepsilon_{ri} \sigma_{ris} + \frac{1}{2} \varepsilon_{\theta i} \sigma_{\theta is} \quad (2.32)$$

And for the outer part, which only consists the rest part of the substrate, its energy equation can be written as

$$dU_{os} = \frac{1}{2} \varepsilon_{ro} \sigma_{ros} + \frac{1}{2} \varepsilon_{\theta o} \sigma_{\theta os} \quad (2.33)$$

Therefore, combing the energy equations of the inner and outer parts, the total energy equations of the whole pressure sensor in the unimorph structure can be determined by using the volume integration in the polarity coordinate system, which is

$$\begin{aligned} U_{total} = & \int_0^{R_p} \int_0^{2\pi} \left( \int_0^{h_p} dU_{ip} dz + \int_{-h_s}^0 dU_{is} dz \right) r d\theta dr \\ & + \int_{R_p}^{R_s} \int_0^{2\pi} \left( \int_{-h_s}^0 dU_{os} dz \right) r d\theta dr \end{aligned} \quad (2.34)$$

The electric filed  $E_3$  can be determined by

$$E_3 = \frac{V}{h_p} \quad (2.35)$$

Where  $V$  is the external voltage on the PZT material. Substituting the equation 2.10, 2.11 and 2.20, the total energy  $U_{total}$  can be expressed as

$$U_{total} = U(P^2) + U(PV) + U(V^2) \quad (2.36)$$

Here the first term describes the mechanical energy and the second term represents the electromechanically coupling energy that can be used to derive the generated voltage. The third term indicates the electric potential energy stored in the PZT disk because its property of capacity when subjected to an external voltage.

The electric charge can be determined by

$$Q_{total} = \frac{dU_{total}}{dV} = \frac{d(U(PV) + U(V^2))}{dV} \quad (2.37)$$

Since in the application of the pressure sensor in unimorph structure, there is no external voltage, thus the generated voltage can be determined from the equation 2.37, which is

$$Q_{gen} = \frac{dU(PV)}{dV} = -\frac{3\pi R_p^2 R_s^3 d_{31} S_{11}^E S_s h_s (h_s + h_p) B_1 S_1 S_2}{2 B_2 B_3} \quad (2.38)$$

Where  $B_1$ - $B_4$  can be found in **Appendix A** and  $S_1$  and  $S_2$  can be obtained by

$$\begin{aligned} S_1 &= S_{11}^E h_s R_s + S_s h_p R_p, \\ S_2 &= 3R_s^2 + \nu_o R_s^2 - R_p^2 - \nu_p R_p^2, \end{aligned} \quad (2.39)$$

For the open-circuit, the capacitance of the PZT disk can be determined by

$$C_p = \frac{\epsilon'_{33} \pi R_p^2}{h_p} \left(1 - \frac{2}{(1 - \nu_i)} \frac{B_4}{B_2} K_{31}^2\right) P \quad (2.40)$$

Where  $K_{31}$  is the electromechanical coupling factor, which is

$$K_{31} = \frac{d_{31}}{\sqrt{\epsilon'_{33} S_{11}^E}} \quad (2.41)$$

Therefore, the voltage collected on the electrodes can be expressed by the ratio of the generated charge  $Q_{gen}$  and the capacitance  $C_p$ , which is

$$V_{gen} = \frac{3 R_s^3 d_{31} S_{11}^E S_s h_s (h_s + h_p) B_1 S_1 S_2}{2 B_2 B_3 \epsilon'_{33} \left(1 - \frac{2}{(1 - \nu_i)} \frac{B_4}{B_2} K_{31}^2\right)} P \quad (2.42)$$

Further, the electric energy converted from the mechanical energy in the pressure become

$$U_{gen} = \frac{1}{2} Q_{gen} V_{gen} \quad (2.43)$$

The sensitivity can also be determined by

$$S_v = \frac{V_{gen}}{P} = \frac{3 R_s^3 d_{31} S_{11}^E S_s h_s (h_s + h_p) B_1 S_1 S_2}{2 B_2 B_3 \epsilon'_{33} \left(1 - \frac{2}{(1 - \nu_i)} \frac{B_4}{B_2} K_{31}^2\right)} \quad (2.44)$$

From the equation 2.29, it can be seen that by optimizing the radius ratio  $R_p/R_s$  and the thickness ratio  $h_p/h_s$ , a higher sensitivity of the sensor can be achieved. To better illustrate the optimization process, a simulated analysis on the sensitivity of the PZT pressure sensor with respect to the radius ratio and the thickness ratio, as shown in Figure 2.9.

From the result, the optimal radius ratio for the PZT pressure sensor is 0.45 and the optimal thickness ratio of that is 1.5. The relating parameters are shown in Table 2-1.

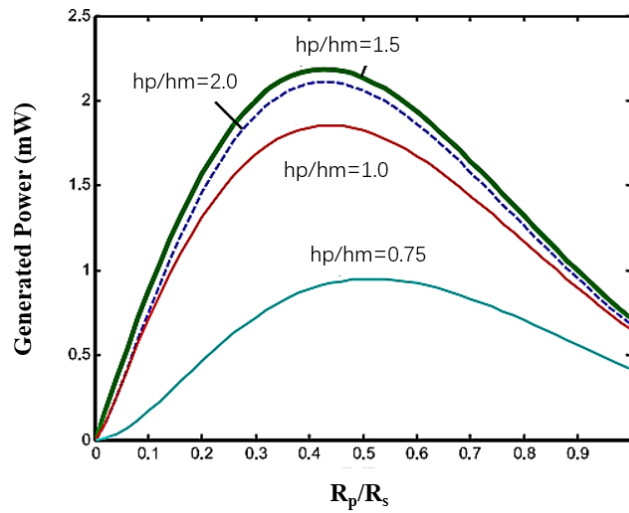


Figure 2.9 Sensitivity performance with different radius ratio and thickness ratio [23]

### 2.4.2 Dynamic Response Analysis

A pressure sensor is electrically equivalent to the equivalent circuit, as shown in Figure 2.10a, which consists of the leakage resistance  $R_p$ , the dielectric capacitance  $C_p$  and the charge source  $Q(t)$  and their relationship can be expressed as

$$Q(t) = K_q Z(t) \quad (2.45)$$

Where the  $K_q$  is the charge generated by per center displacement unit, which can be derived from the equation 2.5 by setting  $r$  equals to zero. Thus, the transfer equation of this system becomes

$$\frac{Q(s)}{P(s)A} = \frac{K_q}{K} \frac{\omega_n^2}{s^2 + 2\xi\omega_n s + \omega_n^2} \quad (2.46)$$

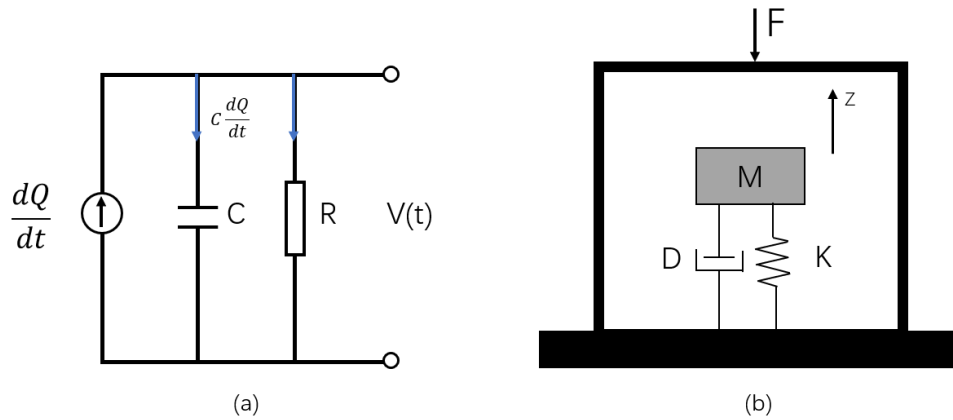


**Figure 2.10 Equivalent model of the pressure sensor: (a) electric model; (b) mechanical model**

Obviously, the equation 2.46 is derived from the mechanical model of the pressure sensor, as shown in Figure 2.10b, where  $A$  is the effective surface area,  $K$  is effective stiffness and  $P$  can be a pulse pressure. The damping ratio  $\xi$  and natural frequency  $\omega_n$  can be determined as

$$\xi = \frac{D}{2\sqrt{KM}} \quad (2.47)$$

$$\omega_n = \sqrt{\frac{K}{M}}$$

By using the Kirchoff's law, the governing equation of the equivalent electric system can be determined as

$$\frac{dQ}{dt} = \frac{K_q dZ}{dt} = C_p \frac{dV}{dt} + \frac{V}{R_p} \quad (2.48)$$

Substituting the time constant  $\tau$ , which equals to the product of the leakage resistance  $R_p$  and the dielectric capacitance  $C_p$ , then applying the Laplace transform, then upper equation becomes

$$\frac{K_q}{C_p} sZ(s) = sV(s) + \frac{V(s)}{\tau} \quad (2.49)$$

$$\frac{V(s)}{Z(s)} = \frac{K_q \tau s}{C_p \tau s + 1} \quad (2.50)$$

Therefore, by substituting the equation 2.49 and 2.50 to the equation 2.46, the dynamic equation of the generated voltage and the applied mechanical pressure can be obtained by

$$\frac{V(s)}{P(s)} = \frac{AK_q}{C_p K} \frac{\omega_n^2}{s^2 + 2\xi\omega_n s + \omega_n^2} \frac{\tau s}{\tau s + 1} \quad (2.51)$$

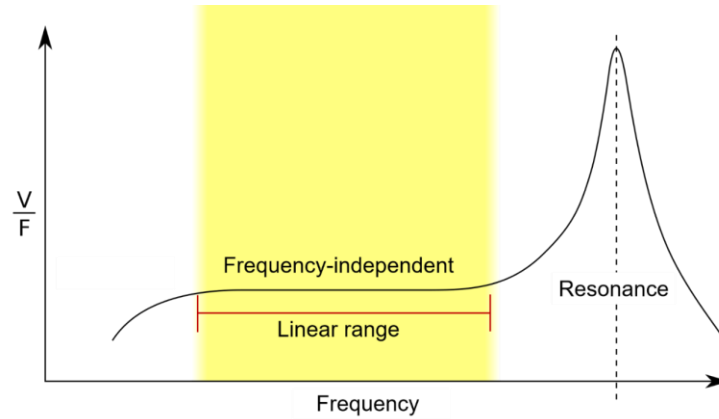


**Figure 2.11 Sensitivity of the sensor is a function of frequency**

By the equation 2.49, it can be seen that the sensitivity  $S_v$  also depends on frequency, as shown in Figure 2.11. Typically,  $S_v$  is measured at the frequency-independent part (the flat segment) of the curve, where there is also called the usable region. The upper limit  $f_u$  of this frequency-independent part is one half of the first resonance frequency and the lower limit of which,  $f_l$ , depends on the leakage resistance  $R_p$  and the dielectric capacitance  $C_p$ :

$$f_l = \frac{1}{2\pi R_p C_p} \quad (2.52)$$

Where the  $R_p$  and  $C_p$  can be determined by

$$\begin{aligned} R_p &= \rho h_p A \\ C_p &= \frac{\varepsilon A}{h_p} \end{aligned} \quad (2.53)$$

Here  $\rho$  is the resistivity of the PZT material and all the other parameters are only determined by the PZT properties. If the frequency of the loading pressure is lower than  $f_l$ , the signal amplitude will greatly reduce, which will cause a relatively large measurement error.

### **3.0 Experimental Study on the Pressure Sensor as a Trigger Switch**

In this chapter, an experiment on the application where the sensor is used as a trigger switch is studied. The experimental principle, related hardware and the system setup will be introduced in section 3.1 and the experimental results and analysis will be discussed in section 3.2, respectively.

#### **3.1 Experimental Principle and Setup**

##### **3.1.1 Experimental Principle**

As mentioned in previous sections, when operating in the generator actions, the piezoelectric ceramic element converts the mechanical energy into electrical energy. Therefore, the sensor device can be used as a trigger to generate an electrical signal as an input to an external circuit. Based on this concept, a universal interface circuit was designed, which can be connected to the previously made pressure sensors to constitute a system. The illustrative block diagram of the whole system is shown in Figure 3.1, where the whole system consists of the system layers and the application layers.

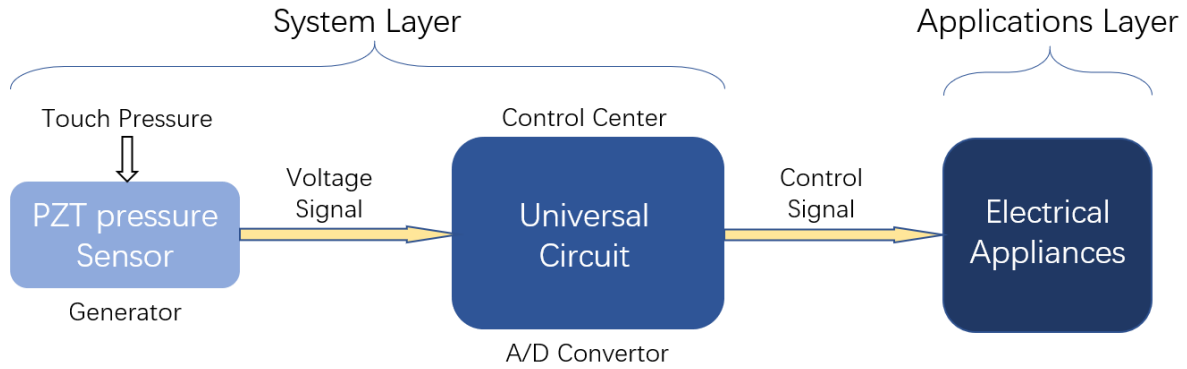


**Figure 3.1 The block diagram of the whole system**

As for the system layer, which is established by connecting the PZT pressure sensor with a multi-functional universal circuit that can be obtained from the market at low price. By using the finger touch to press the PZT pressure sensor, as mentioned in previous sections, a voltage will be generated and received by the circuit. Then, the generated voltage, as an analog signal, will be converted into digital voltage signal by the embedded A/D (analog-digital) converter. Usually, this process can be realized by transform the continuous analog signal into the PWM waves that can be used as a digital signal and the quantities, such as the value of the voltage can be matched to the analog signal by controlling the duty ratio of the PWM waves. Next, this digital signal will be used for judgement and operation in the control program, which will be stored in a microcontroller that can control the electrical appliances, such as the LED, servo motors and so no. For the application layer, according to the differences of the electrical appliances, different control signal will be given by the system layer, which also determines the application case of the experiment.

In this application experiment, a servo motor will be used as the controlled machine to simulate the case using the trigger switch to control the pumps in real life. On the one hand, because the switch is made by the PZT sensor that has a simple and robust structure, which enable the trigger harvesting the features of compact size and high sensitivity at the same time. One the other

hand, the universal circuit and PZT pressure sensors make the whole system become low cost and modular, which is easy to maintain or to replace in the future.

The hardware used in this experiment includes a unimorph PZT pressure sensor fabricated in the previous section, an Arduino UNO board with a power supply module, an 830 tie-points breadboard, an L293D IC chip, a 9V1A adapter, a 3-6V DC motor with a van and several jumper wires. Some of them are introduced as following

The Arduino UNO board

Considering the research objective where a universal circuit is needed for the sensor system and the experiment design where the circuit has both functions of A/D converter and electric appliances controller, the Arduino Uno board, as shown in Figure 3.2, will be an ideal choice.



**Figure 3.2 The Arduino UNO board [26]**

Arduino is an open-source electronics platform based on easy-to-use hardware and software [26]. This platform consists of a board with I/O capabilities and its supplementary program development environments, which enable the developers to use the Arduino board to develop various interactive products. Because of its built-in A/D converter, the board is capable of

reading a large number of signals from sensors and switches, and can also control a variety of physical electrical appliances such as DC motors, lights, etc. The Arduino UNO microcontroller board, which is used in this experiment, is one of the latest Arduino products with the USB interface. It consists of 14 digital input/output ports, 6 analog inputs ports, a USB port, a 16MHz oscillator and an ICSP Header, a power outlet and a reset button. Besides, An ATmega328P chip is used in this board for data conversion from the USB to serial data.

#### Power supply module

Since the DC motor is probably to use more power than an Arduino UNO board can handle directly, to avoid the possibility that the board would be damaged, a power supply module is used in this experiment to solve this potential problem. The power supply module is shown as Figure 3.3 and its specifications are shown in Table 3-1.

**Table 3-1 Product specifications of the Power supply module**

Input voltage:	6.5-9 V (DC) via 5.5 mm*2.1 mm plug
Output voltage:	3.3 or 5V
Maximum output current:	700 mA
Independent Control rail output:	0 V, 3.3 V, 5 V to breadboard
Size:	2.1 in*1.4 in
Indicator type:	LED

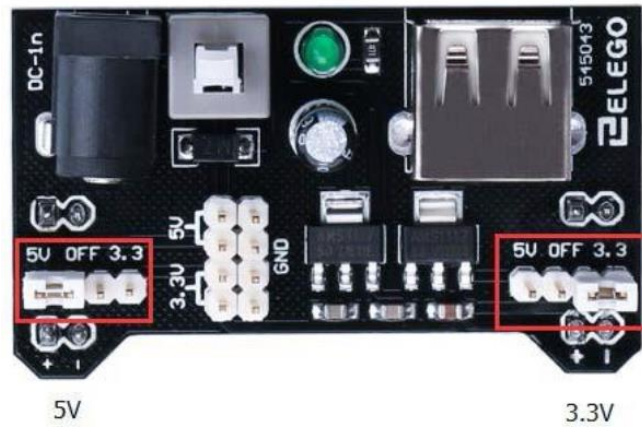


**Figure 3.3 The Power Supply Module**

The L293D IC chip

The L293D is designed to provide bidirectional drive currents of up to 600-mA at voltages from 4.5 V to 36 V. Both devices are designed to drive inductive loads such as relays, solenoids, DC and bipolar stepping motors, as well as other high-current/high-voltage loads in positive supply applications [27]. This Chip is capable of controlling two motors independently. In this experiment, only half of the chip will be used and most of the pins on the right-hand side of this chip are used for controlling another motor.



**Figure 3.4 The L293D IC chip**

### 3.1.2 Experiment Setup

Illustrations of experiment setup are shown in Figure 3.5. The pressure sensor will be connected at the analog port A0 of the Arduino board, where the generated voltage by pressing will be read as an analog signal by the board. On the other side, except the power supply and ground lines of the motor is connected to the L293D directly, the other three lines are connected to the digital port of the Arduino board. In particular, the enable line, which enable the motor to work, is connected to port D5 and the two direction lines that control the motor to rotate in clockwise and counter clockwise are connected to port D4 and D3, respectively. After completing the wire connections, use a USB line to download the program to the Arduino board then use a 9V DC battery to supply the power supply module independently.

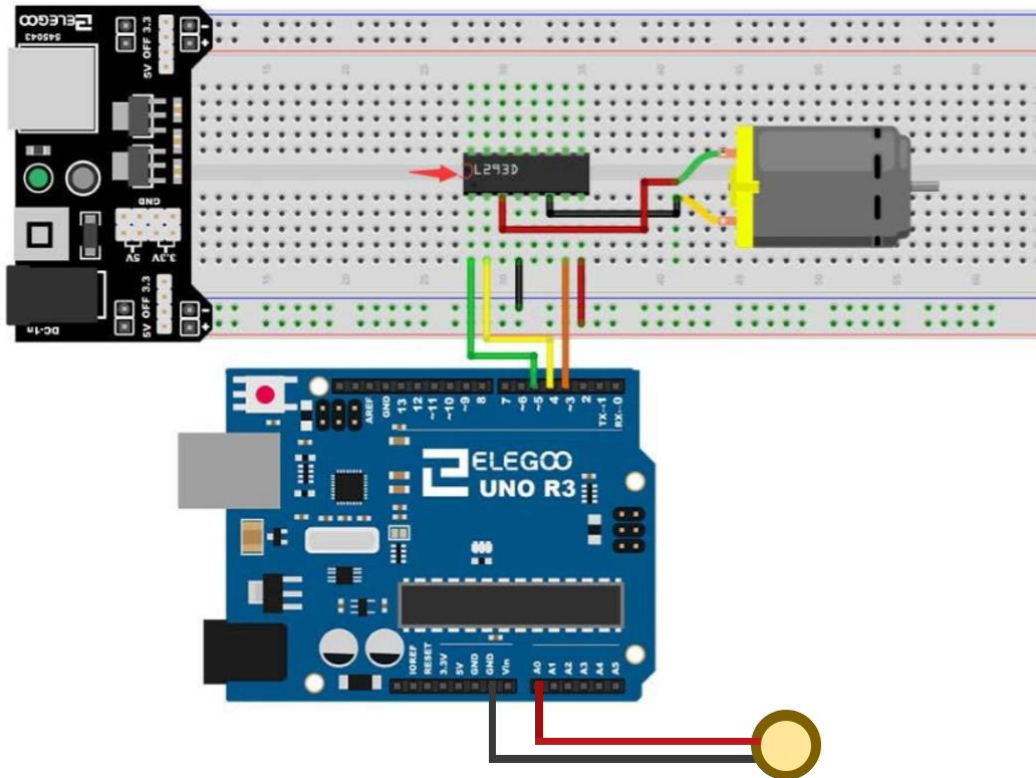
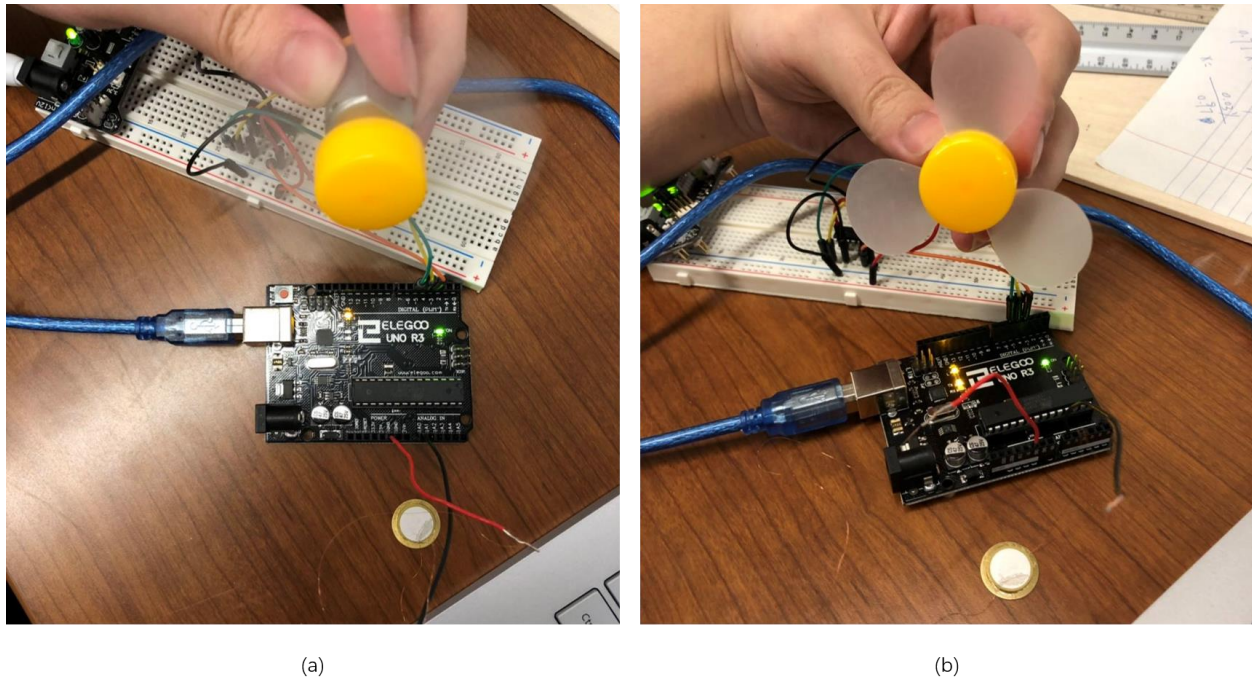


Figure 3.5 The Experiment Setup

The controller program and the studio functions can be found in **Appendix B**.

### 3.2 Experimental Results and Analysis

As shown in Figure 3.6a, after using the finger touch to press the PZT pressure sensor, the DC motor, which was rest state at the beginning, is successfully turned on and drives the fan rotating. Then, by pressing the PZT sensor again, as Figure 3.6b shows, the DC motor was turned off with the fans shutting down.



**Figure 3.6 The Experiment Results: (a) The motor is turned on; (b) The motor is turned off**

These results show that by coordinated processing conducted in the Arduino controller, the PZT pressure sensor can be successfully used as a trigger switch to generate the signal to change the state of the motor. The sensor system is proved to be effective in driving the motor with the power supply module and an appropriate operational amplifier. It is foreseeable that by changing the type of the power supply module and amplifier, a motor with higher power, such as the one used in a pump, can also be driven successfully.

There are two main points in this experiment. One is the manufacturing of the PZT pressure sensor, which has been discussed in detail in last chapter. The other is the design of the controller program.

As shown in the program, to change the state of the motor after pressing the sensor switch every time, a boolean type variable named *Motorstate* was declared and initialized as false. Then, after each time the state of the motor is changed by the voltage signal from the sensor, as shown in Line 24 and 31, the value of this boolean variable will be changed once in order to enter the other branch of this selection structure next time when the voltage signal is detected.

Moreover, considering the time constant of the PZT sensor that will cause the generated voltage to become zero after a delay of time, two key program nodes was set. First, as shown in Line 36, a time delay of the whole program was set. The value of the delay should be set to take into account the response speed of the entire system and the time constant of the sensor. Since the time constant of the PZT sensor used in this experiment is around 1800-2000 ms after the measurement, the time delay of the whole program is set as 1600 ms. Next, a lower limit voltage was declared. One the one hand, this value of the lower limit voltage should not to be too high to avoid the situation where the generated voltage cannot change the status of the motor. One the other hand, the value should also not to be lower than the residual voltage because of the time constant after one-time delay cycle to avoid the situation where the status of the motor was changed even the sensor was not touched.

## 4.0 Experimental Study of the Pressure Sensor as a Dimmer Switch

In this chapter, an experiment on the application where two sensors are used to form a dimmer switch is studied. The experimental principle, related hardware and the system setup will be introduced in section 4.1 and the experimental results and analysis will be discussed in section 4.2, respectively.

### 4.1 Experimental Principle and Setup

#### 4.1.1 Experiment Principle

The objective of this experiment is to use the pressure sensor system to establish a dimmer switch bar that enables people to change the brightness of the light by touching different positions of the switch. This dimmer switch is designed to consist of the unimorph pressure sensors, and a touch bar. The illustrative block diagram of the whole dimmer switch system is shown in Figure 4.1.

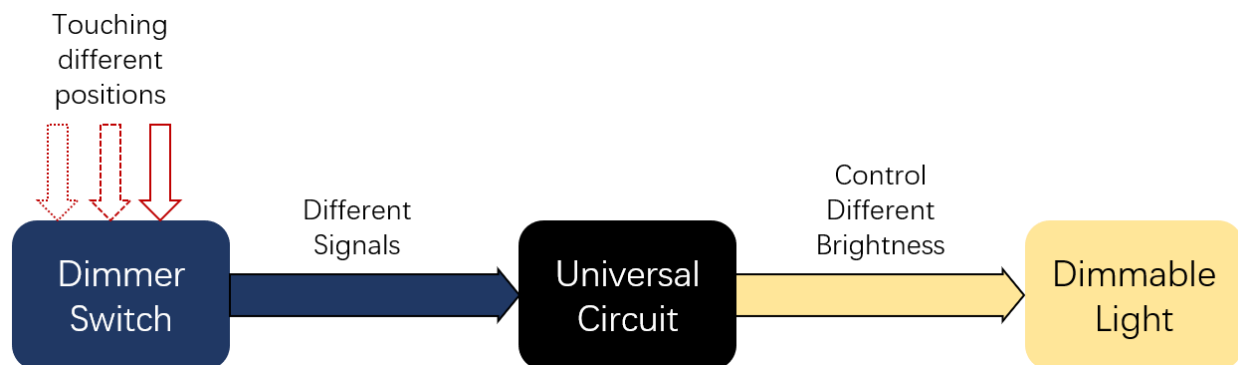
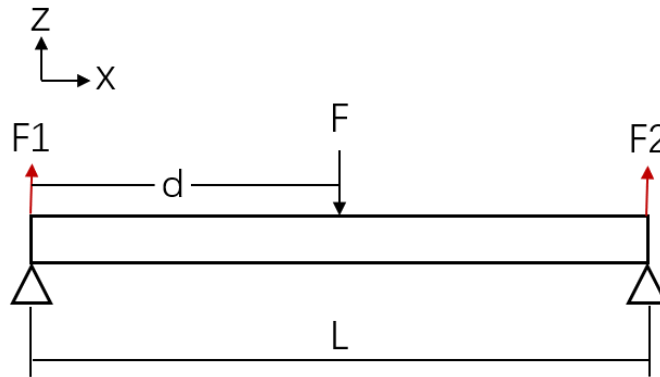


Figure 4.1 The block diagram of the dimmer switch system

Because this dimmer switch is designed to generate different signals according to the differences in the touching position, two requirements need to be satisfied for this dimmer switch. First, the pressure by touching should be converted to the pressure on the pressure sensors. Second, each different signal should correspond to a unique touching position. To satisfy these two requirements, a simple supported bar model was adopted, as shown in Figure 4.2.



**Figure 4.2** The simple supported bar model

In this model, assuming that a bar with the length of  $L$  is stiff enough (no bending in  $z$ -direction) and distance between the touching force  $F$  applied on the bar and the left support end is  $d$ . The reaction force at both ends are  $F_1$  and  $F_2$ , respectively. Therefore, according to the theoretical mechanism, the relationship between  $F$ ,  $F_1$  and  $F_2$  can be determined as

$$\begin{aligned}
 F &= F_1 + F_2 \\
 \frac{F_1}{F_2} &= \frac{(L - d)}{d}
 \end{aligned}
 \tag{4.1}$$

As discussed in the static analysis in section 2.4, since the generated voltage is proportional to the applied force, by combining the equation 2.42 and equation 4.1, the generated voltage at both ends  $V_1$  and  $V_2$  can be determined. Meanwhile, the ratio  $V_1$  to  $V_2$  should also be proportional to the applied force, which can be expressed as

$$\frac{V_1}{V_2} \propto \frac{(L - d)}{d}
 \tag{4.2}$$

According to the equation 4.2, it can be seen that, in this two-end-support structure, the ratio of  $V_1$  and  $V_2$  is only determined by the position of the touching force but not by the magnitude of the force, which greatly simplified the design of the control algorithm because the problem that different people may apply different sized forces when pressing the same position can be

eliminated. In this model, it can also be guaranteed that each touching position will correspond to a unique ratio of  $V_1$  and  $V_2$ , and this ratio will be used as the input signal to the circuit.

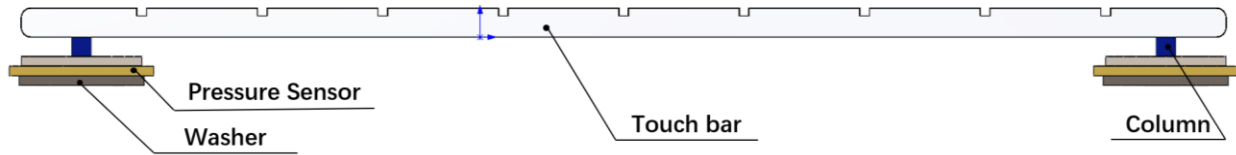


**Figure 4.3 The design of the dimmer switch**

Based on the two-end-support model, the dimmer switch which consists of two unimorph sensors, and 1 plastic touch bar was designed. As shown in Figure 4.3, two PZT pressure sensor with unimorph structure were assigned at both end of the 3D printed plastic touch bar. Each sensor is connected to the bar through a little plastic column, which will transfer the touching pressure to the pressure sensor in a concentrated pressure manner (almost equivalent to the uniform pressure). Through this structure design, the touch pressure will be converted into two partial pressures exerting on the sensors at both ends, respectively. Meanwhile, for each touch, the correspondingly generated voltage  $V_1$  and  $V_2$  can be obtained on both sensors, which makes it possible for the control program to read the ratio of  $V_1$  and  $V_2$  then operate the relative command to adjust the brightness of the light. In addition, in order to prevent unexpected damage to the sensor caused by excessive touch pressure, a washer of a certain thickness is assigned under each of the sensor to limit its bending deflections in z-direction.

The hardware used in this experiment consists of the dimmer switch, an 830 tie-points breadboard, an Arduino UNO board, a  $500\ \Omega$  resistor, an LED and several jumper wires. Among them, the dimmer switch consists of two unimorph PZT pressure sensor fabricated in chapter 2, a 3D printed touch bar with its length, width and thickness of 125mm, 12.5mm and 3mm, respectively, two columns with both the diameter and thickness of 1 mm and two washers with the diameter of 12 mm and thickness of 1 mm.

### 4.1.2 Experiment Setup

Illustrations of experiment setup are shown in Figure 4.4. Since the brightness of the LED is controlled by the voltage applied on it, a function of the Arduino UNO board named *analogWrite* is used, which allows the Arduino to supply a voltage of 0 to 5V that correspond to the number of 0 to 255. Contrary to the *analogRead* function used in the experiment 1, here the *analogWrite* function is using the PWM wave of voltage to match the real analog voltage signal by control the duty cycle. There are 6 ports on the Arduino board with a “~” symbol, indicating that it is a pin that can output PWM signals. The 5mm LED is connected to the pin 10 with a 500  $\Omega$  resistor for current limitation.

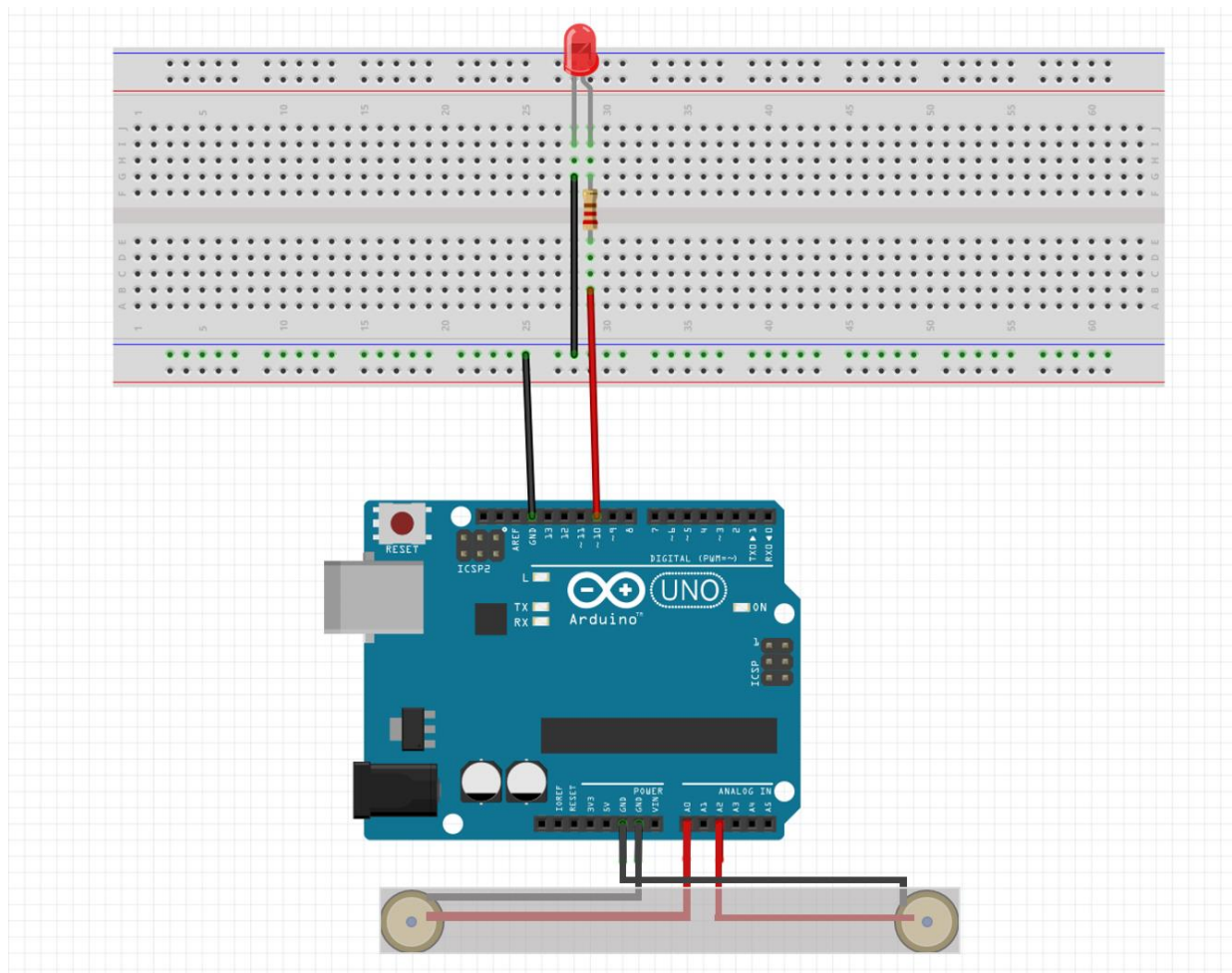


Figure 4.4 The experiment setup

The two unimorph sensors of the dimmer switch are connected to the A0 and A2, respectively. By using the *analogRead* function, the generated voltage V1 and V2 by touch pressing can be obtained by the Arduino board directly and used for the program operation.

The controller program and the studio functions can be found in **Appendix B**.

## 4.2 Experimental Results and Analysis

According to the control program, this dimmer switch is designed to have a 9-level dimming function. In order to illustrate the differences between the brightness levels more clearly, three brightness conditions are shown here to represent the darkest, moderate and brightest condition of the LED, respectively. These three conditions correspond to the left end part, middle part and the right end part of the dimmer switch, respectively, as shown in Figure 4.5.

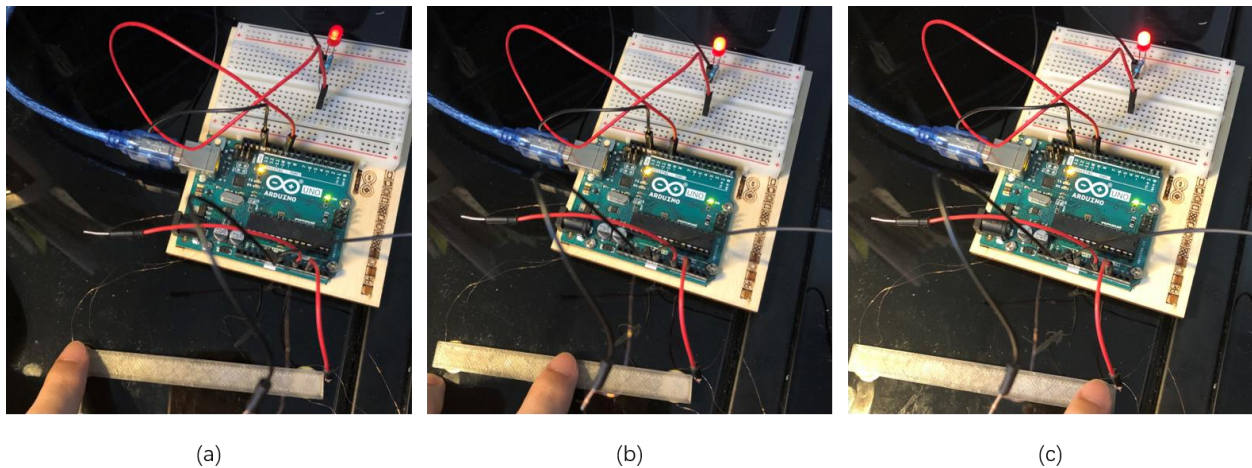


**Figure 4.5 The experiment results: (a) left-end darkest mode; (a) middle moderate mode; (a) right-end brightest mode;**

These results show that by coordinated processing conducted in the Arduino controller, the dimmer switch that consists of two PZT pressure sensors can adjust the brightness of the LED successfully. It is foreseeable that by using some voltage transformers and appropriate amplifier,

a daily used dimmable light, which works at the voltage of 110 volts, can also be controlled and adjusted successfully.

Except for the manufacturing of the PZT pressure sensor, which has been discussed in detail in last chapter, there is another key point of this experiment—the algorithm design of the controller program.

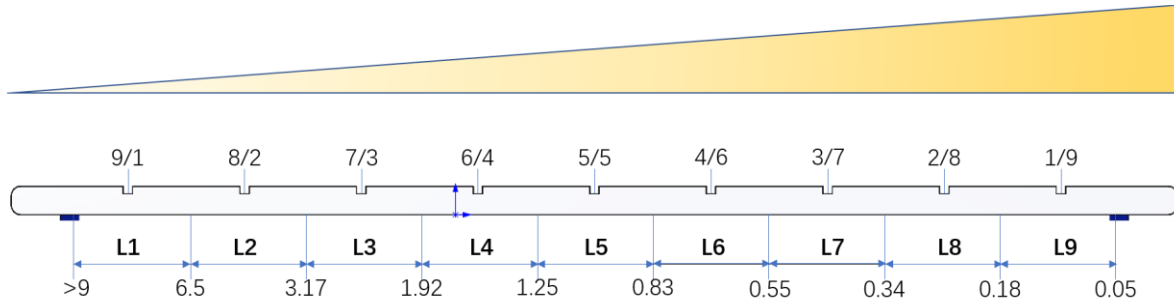


**Figure 4.6 The brightness gradient**

According to the equation 4.2, the ratio of  $V_1$  and  $V_2$  is only determined by the position of the touching force. Therefore, based on the series of the ratios, a brightness gradient can be created, as shown in Figure 4.6. It can be seen that some scale indication notches have been designed according to the ratio of the distance from the groove to the left and right ends. Then, by taking half of the spacing between two adjacent grooves to the left and right sides, the touch bar can be divided into nine blocks corresponding to the nine brightness levels. Next, it is only necessary to calculate the value of ratios corresponding to the two boundaries of different intervals, then the screening conditions corresponding to each brightness level can be determined accordingly, which correspond to the judgement condition of each “if” structure in the control program.

Besides, the problem of the time constant of the PZT pressure sensor is also addressed in this experiment. As shown in Line 38, a time delay of the whole program was set. As for this

experiment, to make sure that each touch position should correspond to a unique ratio of V1 and V2, the value of the delay should be set to match the time constant of the pressure sensor. Only in this way, the voltage generated by last touch operation will not be superimposed to the voltage generated by current touch, thus avoiding the error of the program judgment.

In addition, it needs to point out that the voltage generated by the weight of the touch bar itself should be compensated by setting a negative voltage offset value, as shown in Line 2.

## 5.0 Conclusion and Future Work

### 5.1 Conclusion

The research objective of this thesis is to develop a piezoelectric pressure sensor system which has both the improved sensitivity and simple structure with a universal interface circuit. To achieve this objective, three major parts of work has been done.

First, the PZT piezoelectric pressure sensor was designed and manufactured. By using the tape-casting method, the PZT ceramic element with customized thickness can be fabricated. Then, through the comparison between two most widely used structure designs of the pressure sensors, the PZT pressure sensor using unimorph structure was selected and manufactured. Further, based on this unimorph structure, the theoretical static and dynamic analysis are introduced. For the static analysis, by using the two-part unimorph model, the equation describing the relationship between the pressure and the generated voltage was derived, as well as the sensitivity. For the dynamic analysis, by combing the electric and mechanical equivalent model of the pressure, the relationship between the sensitivity and frequency was discussed.

Second, an experiment where the pressure sensor was used as a trigger switch was studied. This experiment, which is designed for simulating the application that is to drive a pump in real life, is established on the pressure sensor system. In this system, one unimorph pressure sensor was used as a trigger to generate the voltage signal to change the state of motor. Moreover, to convert the analog voltage signal and to control the DC motor, an Arduino UNO board with a power supply module was selected for the circuit part. By appropriately adjusting the relevant parameters in the control program, the experiment successfully achieved the object that using the pressure sensor as a trigger switch to change the working state of the motor.

Third, another experiment where the pressure sensors were used as a dimmer switch was studied. This experiment is designed for creating a novel dimmer switch that enable people to adjust the brightness of the light by touching different positions on the switch. This experiment is also established on the pressure sensor system. In this system, two unimorph pressure sensor were placed at the two ends of the switch as voltage generators. Once the position of the touch is changed,

the voltage generated by the two sensors also changed. The Arduino UNO board was also selected for the circuit part in this system. Based on the relationship between position of the force and the generated voltages, by appropriately setting brightness interval corresponding to different positions, the experiment successfully achieved the object that using the pressure sensors to form a dimmer switch to adjust the brightness of the light.

## **5.2 Future Work**

In both experiments, time constant of the PZT material is a problem to be addressed. To match time for the generated voltage to attenuate to zero, the total delay time of the control program has to be adjusted manually. Meanwhile, this delay also more or less makes the response of the whole system become not very rapid. To solve this problem, a specialized cutoff circuit or a time window which can only reserve the peak value of the generated voltage and filter the rest of that can be developed in the future work.

For the further application on this pressure sensor system, an experiment which uses three or four pressure sensors to form a two-dimensional pad can be designed in the future work. This pad probably can generate different command to control the electric appliances according to different touching positions.

## Appendix A Mathematical Derivation for Static Response Analysis

### A.1 EXPANSION OF THE SYMBOLS USED IN THE STATIC ANALYSIS

$$C_0 = (-R_s^2 v_i + R_p^2 v_i - R_p^2 - R_s^2) D_i + (R_s^2 v_i - R_p^2 v_i + R_p^2 - R_s^2) D_o$$

$$C_1 = -\frac{P_0}{64} \frac{R_1^6}{D_i D_o C_0} \left( ((v_i - 1) + (3 - v_i) + 4(1 + v_i) \ln\left(\frac{R_s}{R_p}\right) + 12 \ln(R_s)) \left(\frac{R_s}{R_p}\right)^2 - ((v_i + 7) + 12 \ln(R_p) + 4v_i \ln\left(\frac{R_s}{R_p}\right)) \left(\frac{R_s}{R_p}\right)^4 + (v_i + 5) \left(\frac{R_s}{R_p}\right)^6 (D_i^2 + (2(1 - v_i) - \left(4(v_i + 1) \ln\left(\frac{R_s}{R_p}\right) - 2(v_i - 2) \left(\frac{R_s}{R_p}\right)^2 + (4(v_i + 3) \ln\left(\frac{R_s}{R_p}\right) + (v_i + 7)) \left(\frac{R_s}{R_p}\right)^4 - (v_i - 5) \left(\frac{R_s}{R_p}\right)^6) D_i D_o + (v_i - 1) \left(1 - \left(\frac{R_s}{R_p}\right)^2\right) D_o^2) \right)$$

$$C_2 = -\frac{P_0}{32} \frac{R_1^4}{(v_i + 1) D_i C_0} \left( (1 - v_i^2) \left(\left(\frac{R_s}{R_p}\right)^2 - 1\right) - (1 + 2v_i) \left(\frac{R_s}{R_p}\right)^4 - (1 - v_i^2) \left(\left(\frac{R_s}{R_p}\right)^2 - 1\right) D_o \right)$$

$$C_3 = -\frac{P_0}{64} \frac{R_1^4 R_2^2}{D_o C_0} \left( (v_i + 1) (2(1 - v_i) + 4(1 + v_i) \ln\left(\frac{R_s}{R_p}\right) - ((1 - v_i) + 4(v_i + 3) \ln(R_s)) \left(\frac{R_s}{R_p}\right)^2 + (v_i + 5) \left(\frac{R_s}{R_p}\right)^4) D_i + (2(v_i^2 - 1) - 4(v_i + 1)^2 \ln(R_s) + ((1 - v_i^2) + 4(v_i + 1)(v_i + 3) \ln(R_p) \left(\frac{R_s}{R_p}\right)^2 - (v_i - 1)(v_i + 5) \left(\frac{R_s}{R_p}\right)^2) D_o \right)$$

$$C_4 = \frac{P_0}{16} \frac{R_1^2 R_2^2}{D_o C_0} (-R_s^2 v_i + v_i R_p^2 - 3R_s^2 + R_p^2) (D_i - D_o)$$

$$C_5 = -\frac{P_0}{32} \frac{(-R_s^4 v_i + R_p^4 v_i - 3R_s^4 - R_p^4) ((1 + v_i) D_i - (v_i - 1) D_o)}{(v_i + 1) D_o C_0}$$

$$B_1 = (-h_p^4 s_s^2 + 6s_{11}^E s_s h_p^2 h_m^2 + 4s_{11}^E s_s h_m h_p (h_m^2 + h_p^2) + h_m^4 s_{11}^{E2})$$

$$B_2 = (2h_p^4 s_s^2 s_{11}^E R_s h_m R_p + 4s_{11}^{E2} s_s h_p^3 h_m^2 R_s^2 + h_p^5 s_m^3 R_p^2 + 2h_m^4 s_{11}^{E2} R_s h_p R_p s_s + 4s_{11}^E R_p^2 h_m^3 h_p^2 s_s^2 + h_m^5 s_{11}^{E3} R_s^2 + 3h_p s_s h_m^4 s_{11}^{E2} R_s^2 + 6h_p^2 s_s h_m^3 s_{11}^{E2} R_s^2 + 3h_m s_s^2 h_m^4 s_{11}^E R_p^2 + 6h_m^2 s_s^2 h_p^3 R_p^2)$$

$$B_3 = R_s^2 (s_{11}^E s_s (6h_p^2 h_m^2 + 4h_p^3 h_m + 5h_m^3 h_p + 3v_o h_m^3 h_p + 4v_o h_p^3 h_m + 6v_o h_p^2 h_m^2) + v_o h_p^4 s_s + h_p^4 s_s^2) \\ + 2h_m^4 s_{11}^{E2} - R_p^2 h_p s_s (v_o - 1) (h_p^3 s_s + 4h_p^2 h_m s_{11}^E R_s^2 + 3h_m^3 s_{11}^E + 6s_{11}^E h_m^2 h_p)$$

$$B_4 = 6s_{11}^E s_s^2 h_p^2 h_m^2 R_s^2 + 2s_{11}^E R_s h_p^4 R_p h_m s_s^2 + s_{11}^{E3} R_s^2 h_m^5 + s_{11}^{E2} R_s^2 s_s 5h_p^3 h_m^2 + 2s_{11}^{E2} R_s R_p h_m^4 h_p s_s \\ + h_p^5 R_p^2 s_s^3 + 3s_{11}^E s_s^2 R_p^2 h_p^2 h_m^3$$

$$\kappa_{ri} = -\frac{12s_{11}^E s_s (s_{11}^E h_m R_s + s_s h_p R_p)^2}{B_2} (M_{ri} - v_i M_{\theta i}) \\ + \frac{6d_{31} s_{11}^E s_s h_p h_m (s_{11}^E h_m R_s + s_s h_p R_p) R_s (h_m + h_p)}{B_2} E_3$$

$$\kappa_{\theta i} = -\frac{12s_{11}^E s_s (s_{11}^E h_m R_s + s_s h_p R_p)^2}{B_2} (M_{\theta i} - v_i M_{ri}) \\ + \frac{6d_{31} s_{11}^E s_s h_p h_m (s_{11}^E h_m R_s + s_s h_p R_p) R_s (h_m + h_p)}{B_2} E_3$$

$$\kappa_{ro} = -\frac{12s_{11}^E s_s (s_{11}^E h_m R_s + s_s h_p R_p)^2}{B_1 h_m} (M_{ro} - v_o M_{\theta o})$$

$$\kappa_{\theta o} = -\frac{12s_{11}^E s_s (s_{11}^E h_m R_s + s_s h_p R_p)^2}{B_1 h_m} (M_{\theta o} - v_o M_{ro})$$

## Appendix B Control Program for the Two Experiments

### B.1 Control Program for experiment 1

```
#define ENABLE 5

#define DIRA 3

#define DIRB 4

boolean MotorState = false; // indicating LED state

void setup()

{

  pinMode(ENABLE, OUTPUT);

  pinMode(DIRA, OUTPUT);

  pinMode(DIRB, OUTPUT);

}

void loop()

{

  int V1 = analogRead(A0);

  float vol1 = V1 * (10.0 / 1024);

  if (vol1 > 3.20)

  {

    if (MotorState == true)
```

```

{
    digitalWrite(ENABLE, LOW); //enable on
    MotorState = !MotorState;
}
else
{
    digitalWrite(ENABLE, HIGH); //enable on
    digitalWrite(DIRA, HIGH); //one way
    digitalWrite(DIRB, LOW);
    MotorState = !MotorState;
}
}
else
{}
delay(1600);
}

```

## B.2 Control Program for experiment 2

```

#define LED 10
#define Offset -2.37
void setup() {

```

```

Serial.begin(9600);

pinMode(LED, OUTPUT);

}

void loop() {

  int V1 = analogRead(A0);

  int V2 = analogRead(A2);

  float vol1 = V1 * (10.0 / 1024) + Offset;

  float vol2 = V2 * (10.0 / 1024) + Offset;

  float r = vol1 / vol2;

  if (r > 9)

  {

    analogWrite(LED, 55);

  }

  if (r < 9 && r >= 6.50)

  {

    analogWrite(LED, 75);

  }

  if (r < 6.50 && r >= 3.17)

  {

    analogWrite(LED, 95);

  }

  if (r < 3.17 && r >= 1.92)

```

```
{
    analogWrite(LED, 115);
}
if (r < 1.92 && r >= 1.25)
{
    analogWrite(LED, 135);
}
if (r < 1.25 && r >= 0.83)
{
    analogWrite(LED, 155);
}
if (r < 0.83 && r >= 0.55)
{
    analogWrite(LED, 175);
}
if (r < 0.55 && r >= 0.34)
{
    analogWrite(LED, 195);
}
if (r < 0.55 && r >= 0.18)
{
    analogWrite(LED, 215);
}
```

```
if (r < 0.13 && r >= 0.05)
{
    analogWrite(LED, 235);
}
if (r < 0.05)
{
    analogWrite(LED, 255);
}
delay(2000);
}
```

## Bibliography

1. Antonio Arnau, et al. "Piezoelectric Transducers and Applications". Springer-Verlag, Berlin Heidelberg, 2008
2. S. O. R. Moheimani, et al. "Piezoelectric Transducers for Vibration Control and Damping", Springer, London, UK, 2006.
3. G. Lippmann, "Principe de conservation de l'électricité" Annales de Physique et de Chimie", 5<sup>a</sup>Serie 24: 145-178, 1881
4. Walter Heywang, et al. "Piezoelectricity". Springer-Verlag, Berlin Heidelberg, 2008
5. Ian R. Henderson, et al. "Piezoelectric Ceramics: Principles and Applications". APC Internation Ltd., Mackeyville, PA, 2002
6. A Muliana, "Time dependent behavior of ferroelectric materials undergoing changes in their material properties with electric field and temperature". International Journal of Solids and Structures 48 (19), 2718-2731
7. W. Voigt, "Lehrbuch der Kristallphysik". B.G. Teubner, Leipzig, 1928
8. <https://en.wikipedia.org/wiki/Piezoelectricity>
9. <https://en.wikipedia.org/wiki/Transducer>
10. Fraden J., et al. "Handbook of Modern Sensors", American Institute of Physics Press, Woodbury, NY, 1997.
11. [https://en.wikipedia.org/wiki/Piezoelectric\\_sensor](https://en.wikipedia.org/wiki/Piezoelectric_sensor)
12. [http://www.pcb.com/TechSupport/tech\\_gen](http://www.pcb.com/TechSupport/tech_gen)
13. <https://www.ctscorp.com/products/piezoelectric-products/>
14. <https://www.kistler.com/en/products/components/pressure-sensors/>
15. <https://www.bdsensors.de/en/pressure/piezoelectric-pressure-sensors/>
16. Qin, Lifeng, et al. "Fabrication and characterization of thick-film piezoelectric lead zirconate titanate ceramic resonators by tape-casting." Ultrasonics, Ferroelectrics and Frequency Control, IEEE Transactions on 59.12 (2012): 2803-2812

17. Rongjie Liang, 'Piezoelectric pressure sensor based on PZT thick film composite device', Master Thesis, Dept. of Mechanical and Material Science, University of Pittsburgh, December 2014
18. T. Bailey, et al. "Distributed piezoelectric-polymer active vibration control of a cantilever", AIAA J. Guidance Contr., Vol.6, pp. 605-611,1985
19. Y. Sugawara, et al. "Metal-ceramic composite actuators", J. Amer. Cerm. Soc, Vol. 75, No. 4, pp.996-998, 1992
20. Y. Liao, et al. "Model of a single mode energy harvester and properties for optimal power generation". Smart Materials and Structures. 17 (6) (2008) 065026.
21. R. Xu, et al. "Screen printed PZT/PZT thick film bimorph MEMS cantilever device for vibration energy harvesting". Sensors and Actuators A, 188 (2012) 383–388
22. Lim, C.W. "Three Dimensional Electromechanical Responses of a Parallel Piezoelectric Bimorph". International Journal of Solids and Structures, 38(16):2833-2849, 2001
23. Mo, Changki, Leon J. Radziemski, and William W. Clark. "Analysis of piezoelectric circular diaphragm energy harvesters for use in a pressure fluctuating system." Smart Materials and Structures 19.2 (2010): 025016.
24. Vinson JR (1974) Structural Mechanics: The Behavior of Plates and Shells. John Wiley & Sons New York
25. R.M. Christensen, Mechanics of Composite Materials, Wiley, New York, 1979.
26. <https://store.arduino.cc/usa/arduino-uno-rev3>
27. <http://www.ti.com/lit/ds/symlink/l293.pdf>